UNIVERSITAT POLITÈCNICA DE VALÈNCIA

grupo de HIDROGEOLOGIA

Escuela Técnica Superior de Ingenieros de Caminos, Canales y Puertos

Departamento de Ingeniería Hidráulica y Medio Ambiente

Master Theses

Máster Universitario en Hidráulica y Medio Ambiente

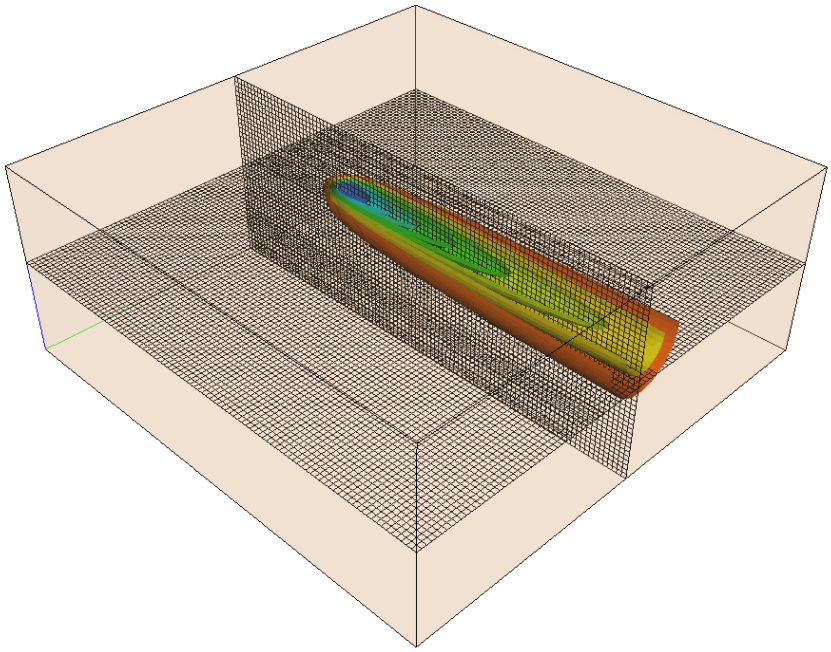

EVALUATION OF THE INFLUENCE OF HETEROGENEITY ON HEAT TRANSPORT SIMULATIONS IN SHALLOW GEOTHERMAL SYSTEMS. APPLICATION ON A FIELD SITE

Max Reisinger

Valencia, July 2011

EVALUATION OF THE INFLUENCE OF HETEROGENEITY ON HEAT TRANSPORT SIMULATIONS IN SHALLOW GEOTHERMAL SYSTEMS. APPLICATION ON A FIELD SITE

Escuela Técnica Superior de Ingenieros de Caminos, Canales y Puertos

Departamento de Ingeniería Hidráulica y Medio Ambiente

Master Theses

Max Reisinger

Supervisor:

Javier Rodrigo Ilarri

Valencia, July 2011

Statement

I hereby certify that the work presented here was conducted solely by myself and with the references listed.

Valencia, July 2011

Abstract

Global warming and the narrowness of fossil fluids have led to an increasing global demand for renewable energy sources. Geothermal energy is one of these renewable energies which uses the heat stored under earth surface to produce electricity, heat and cool buildings and provide heat for a variety of industrial processes. The most common system to extract heat from the underground in shallow geothermal systems is the Ground Source Heat Pump system (GSHP).

In the present work, a 3 dimensional model was developed to simulate heat transport in a Shallow Geothermal system considering an open loop system. The model consists in a 3D grid with the dimensions 100x100x40. Cold water is injected with a partially penetrating injection well at a constant rate. MT3DMS was used as heat transport code to perform 360 days steady state simulations. The model layout, flow and transport parameters are based on a report on a test field site in Germany.

The main objective of this work was to evaluate the influence of the heterogeneity of parameters such as permeability, porosity and thermal conductivity on heat transport simulations. Stanford Geostatistical Modeling Software (SGeMS) was used to create syntactical aquifer models simulating different degrees of heterogeneity in the hydraulic conductivity fields. An overall of 61 simulations have been made using the PMWIN package.

In a first step heat transport simulations for the heterogenic hydraulic conductivity fields were made keeping the porosity and thermal conductivity constant. In the second step heterogenic fields for all parameters (k, n, ρ_b, λ heterogeneous) were created and introduced to the model. The simulations of all scenarios are compared to each other and to a homogeneous reference case to evaluate the influence of heterogeneity.

The heterogeneity of the hydraulic conductivity showed to have a significant influence on the evaluation of a cold plume in a porous media. Higher variances in the hydraulic conductivity distributions cause an important rise in the variability of the simulated temperature fields and a considerable uncertainty in the simulated heat distribution in the aquifer system.

The heterogeneity of porosity and thermal conductivity seems to be less important than the one of permeability. Anyhow higher degrees of heterogeneity show slight differences between the simulations made with homogenous and heterogeneous porosity and thermal conductivity. In the most heterogeneous case ($\sigma^2_{logk}=1$) the calculated variance increases considerably introducing the calculated porosity and thermal conductivity fields.

Resumen

El Calentamiento global y la escasez de combustibles fósiles conllevan a un aumento en la demanda global de energías renovables. La energía geotérmica es una de estas fuentes de energía alternativa. Ésta se aprovecha de la energía térmica almacenada debajo de la superficie de la tierra para la producción electricidad, la calefacción de edificios y para el suministro de calor en procesos industriales. En sistemas geotérmicos de poca profundidad el sistema de extracción de calor más utilizado es la bomba de calor.

En este trabajo, fue creado un modelo 3D con el fin de simular el transporte de calor en un sistema geotérmico de poca profundidad considerando un circuito cerrado. El modelo consiste en una malla 3D con las dimensiones 100x100x40 metros. El agua fría es inyectada a través de de un pozo de inyección con un caudal constante. El MT3DMS fue utilizado como código de transporte para llevar a cabo simulaciones de 360 días en estado estacionario. La configuración del modelo y también los parámetros de flujo y transporte fueron elegidos considerando un informe sobre un campo de ensayo situado en Alemania.

El objetivo principal de este trabajo es la evaluación de la influencia de heterogeneidad de parámetros como la conductividad hidráulica, la porosidad y la conductividad térmica sobre la simulación del transporte de calor. El programa Stanford Geostatistical Modeling Software (SGeMS) fue utilizado para crear modelos de acuíferos sintéticos con diferentes grados de heterogeneidad. En conjunto 61 simulaciones de transporte de calor fueron realizados utilizando el software PMWIN.

En un primer paso se hicieron simulaciones para campos heterogéneos de conductividad hidráulica manteniendo la porosidad y conductividad térmica constante. En un segundo paso se introdujeron campos heterogéneos para todos los parámetros (k, n, ρ_b, λ heterogéneo) al modelo para realizar otras simulaciones. Las simulaciones de todos los escenarios fueron luego comparadas para evaluar la importancia de la heterogeneidad de los diferentes parámetros.

Los resultados demuestran que la heterogeneidad de la conductividad hidráulica tiene efectos importantes sobre la evaluación de una pluma de calor en un medio poroso. Una subida del grado de heterogeneidad resulta en un aumento de la variabilidad de la distribución de la temperatura y una considerable incertidumbre en la predicción de la evaluación de la pluma de calor.

La heterogeneidad de la porosidad y la conductividad térmica parecen ser menos importantes que la conductividad hidráulica. Sin embargo, altos grados de heterogeneidad provocaron ciertas diferencias entre las simulaciones realizadas con porosidad y conductividad térmica homogénea y las de porosidad y conductividad térmica heterogénea.

Resum

El calfament global i l'escassetat de combustibles fòssils comporten a un augment en la demanda global d'energies renovables. L'energia geotèrmica és una d'estes fonts d'energia alternativa. Aquesta s'aprofita de l'energia tèrmica emmagatzemada davall de la superfície de la terra per a la producció electricitat, la calefacció d'edificis i per al subministrament de calor en processos industrials. En sistemes geotèrmics de poca profunditat el sistema d'extracció de calor més utilitzat és la bomba de calor.

En aquest treball, es va crear un model 3D a fi de simular el transport de calor en un sistema geotèrmic de poca profunditat considerant un circuit tancat. El model consistix en una malla 3D amb les dimensions 100x100x40 metres. L'aigua freda és injectada a través de d'un pou d'injecció amb un cabal constant. El MT3DMS va ser utilitzat com a codi de transport per a dur a terme simulacions de 360 dies en estat estacionari. La configuració del model i també els paràmetres de flux i transport van ser triats considerant un informe sobre un camp d'assaig situat a Alemanya.

L'objectiu principal d'este treball és l'avaluació de la influència d'heterogeneïtat de paràmetres com la conductivitat hidràulica, la porositat i la conductivitat tèrmica sobre la simulació del transport de calor. El programa Stanford Geostatistical Modeling Programari (SGeMS) va ser utilitzat per a crear models d'aqüífers sintètics amb diferents graus d'heterogeneïtat. En conjunt 61 simulacions de transport de calor van ser realitzats utilitzant el programari PMWIN.

En un primer pas es van fer simulacions per a camps heterogenis de conductivitat hidràulica mantenint la porositat i conductivitat tèrmica constant. En un segon pas es van introduir camps heterogenis per a tots els paràmetres (k, n, ρ_b, λ heterogeni) al model per a realitzar altres simulacions. Les simulacions de tots els escenaris van ser després comparades per a avaluar la importància de l'heterogeneïtat dels diferents paràmetres.

Els resultats demostren que l'heterogeneïtat de la conductivitat hidràulica té efectes importants sobre l'avaluació d'una ploma de calor en un mitjà porós. Una pujada del grau d'heterogeneïtat resulta en un augment de la variabilitat de la distribució de la temperatura i una considerable incertesa en la predicció de l'avaluació de la ploma de calor.

L'heterogeneïtat de la porositat i la conductivitat tèrmica pareixen ser menys importants que la conductivitat hidràulica. No obstant això, alts graus d'heterogeneïtat van provocar certes diferències entre les simulacions realitzades amb porositat i conductivitat tèrmica homogènia i les de porositat i conductivitat tèrmica heterogènia.

Table of contents

Nomenclature

Symbol	Unit	Description
A	$[m^2]$	Area
c	$[J\ kg^{-1} K^{-1}]$	Specific heat capacity
C	$[kg\ m^{-3}]$	Dissolved mass concentration
$C_{C\text{-}K}$	[-]	Kozeny-Carman empirical coefficient
c_f	$[J\ kg^{-1} K^{-1}]$	Specific heat capacity fluid
c_s	$[J\ kg^{-1} K^{-1}]$	Specific heat capacity solid
C_s	$[kg\ m^{-3}]$	Concentration sources and sinks
c_w	$[J\ kg^{-1} K^{-1}]$	Specific heat capacity of water
d	[m]	Diameter of the grain
D_{ij}	[-]	Dispersion coefficient
D_m	$[m^2\ s^{-1}]$	Coefficient of molecular diffusion
e	[-]	Void ratio
F	[m]	Depth of the water table
H	[m]	Thickness of the aquifer
i	[-]	Hydraulic gradient
J	$[kg\ s^{-1} m^{-2}]$	Diffusion flux
J_H	$[W\ m^{-2}]$	Heat flux
k	$[m\ s^{-1}]$	Hydraulic conductivity
K_d	$m^3\ kg^{-1}$	Distribution coefficient
n	[-]	Effective porosity
n_t	[-]	Total porosity
Q	$[m^3\ s^{-1}]$	Mean water injection rate
q_h	$[W\ m^{-3}]$	Heat injection or extraction
q_s	$[m^3\ s^{-1}\ m^{-3}]$	Flow rate of sources and sinks solute transport
r	$[s^{-1}]$	Reaction rate constant for the dissolved phase
R	[-]	Retardation factor
S_0	$[c\ m^{-1}]$	Specific surface area per unit volume of particles
t	[s]	Simulated time periode
T_0	[K]	Initial temperature
T_{ab}	$[m^2\ s^{-1}]$	Transmissivity
T_f	[K]	Temperature of the water
T_{in}	[K]	Temperature of the injected water
T_s	[K]	Temperature of the solid
v_a	$[m\ s^{-1}]$	Seepage velocity

V_t	$[m^3]$	Total volume
V_v	$[m^3]$	Volume of voids
V_{vi}	$[m^3]$	Volume of interconnected voids
α_H	$[m]$	Horizontal transverse dispersivity coefficient
α_H	$[m]$	Vertical transverse dispersivity coefficient
α_L	$[m]$	Longitudinal dispersivity coefficient
α_s	$[m]$	Dispersivity coefficient
γ	$[-]$	Unit weight of the fluid
λ	$[W\ m^{-1}\ K^{-1}]$	Thermal conductivity
λ_e	$[W\ m^{-1}\ K^{-1}]$	Overall thermal conductivity of the saturated aquifer
λ_f	$[W\ m^{-1}\ K^{-1}]$	Thermal conductivity fluid
λ_s	$[W\ m^{-1}\ K^{-1}]$	Thermal conductivity solid
μ	$[kg\ s^{-1}\ m^{-1}]$	Viscosity of the fluid
ν_s	$[m\ s^{-1}]$	Velocity
ρ_b	$[kg\ m^{-3}]$	Bulk density
$\rho_e c_e$	$[Jm^{-3}K^{-1}]$	Volumetric heat capacity of the saturated aquifer
ρ_f	$[kg\ m^{-3}]$	Density of water
$\rho_f c_f$	$[Jm^{-3}K^{-1}]$	Volumetric heat capacity of the fluid
ρ_s	$[kg\ m^{-3}]$	Density of the solid
$\rho_s c_s$	$[Jm^{-3}K^{-1}]$	Volumetric heat capacity of the solid
σ^2	$[-]$	Variance

List of Images

List of Tables

1. INTRODUCTION

Global warming and the narrowness of fossil fluids have led to an increasing global demand of renewable energy sources. Renewable energy resources, such as wind, solar, hydropower and geothermal energy offer clean alternatives for a sustainable energy supply.

According to a report from the Renewable Energy Policy Network for the 21st Century, renewable energy must play a major role in the global energy supply to meet the increasingly serious environmental and economic threats of climate change.

The report's lead author, John Christensen from the UNEP Risoe Centre on Climate, Energy and Sustainable Development, says that many renewable energy technologies have "moved from being a passion for the dedicated few to a major economic sector attracting large industrial companies and financial institutions" (Christensen, 2006)

Geothermal energy is one of these renewable energies and which can be used to produce electricity, heat and cool buildings and provide heat for a variety of industrial processes. The term “Geothermal Energy” describes all forms of heat stored under earth surface. Geothermal energy is continuously available all over the planet although available temperatures vary considerably. Highest temperatures can be found at edges of tectonic plates and over “Hot Spots” where temperature gradients are much higher than in other parts (Armstrong & Blundell, 2007).

Geothermal energy is one of the oldest energy sources and humans have used it for many years. Already 1600 b.C. Roman, Chinese and Japanese civilizations used natural hot springs for bathing, cooking and heating. In 1892 the United States first geothermal district heating system was established in Boise/Idaho. In 1913 the Italian scientist Piero Ginori Conti invented the first geothermal electric power plant (Gleason, 2008).

Geothermal energy is divided in low, medium and high temperature resources. Traditionally, mean temperature resources in the range of 40℃ to 150℃ have been used directly for heating and bathing or in the process industry. High temperature sources with temperatures above 150℃ can be used for electricity generation and industrial processes. The low temperature resources are usually obtained at a shallow depth of up to 300 meters below the earth surface. They are mostly used for building heating and cooling as well as for hot water supply (Armstrong & Blundell, 2007).

1.1. Shallow geothermal systems

Shallow geothermal system use the energy stored in the first approximately 400 m under the earth surface (LLOPIS TRILLO & LÓPEZ JIMENO, 2009). From about 10-20 m in depth, the temperature is considered to be constant during the year and with further depth temperatures are increasing according to the geothermal gradient (average 3℃ for each 100 m of depth) (Sanner, 2001).

Due to the low temperatures (10 ℃ to max. 30 ℃) i n the shallow zone, the obtained energy is called low enthalpy energy. Low enthalpy energy can´t be used directly. Geothermal systems have to be applied to make use of it.

The most common system to extract heat from the underground is the Ground Source Heat Pump system (GSHP). A GSHP system extracts thermal energy from a cold zone to transport it to a warmer zone. The natural form of heat transport would be in the other direction (from warm to cold) according to the second law of thermodynamics. To invert the natural heat flow, it is necessary to supply the system with energy, normally with a compressor. In this form for each kWh of electric energy used for the compressor, up to 4.5 kWh of thermal energy can be provided (Conde Lázaro & Ramos Millán, 2009). Another advantage of GSHP´s is the reversibility which permits heating and cooling with the same system.

A ground source heat pump system consists of two parts: an outdoor piping system outside the house as heat source and the heat pump unit inside the house. The ground loop provides heat to the system. Because of the low temperatures, the fluid of the ground loop can´t be used directly. Passing through a primary heat exchanger (evaporator) the heat is transferred from the ground loop to the refrigerant fluid which circulates in the heat pump unit (Canada, 2009).

The refrigerant is a fluid which evaporates at low temperatures forming a low temperature vapor. So the heat is absorbed in form of latent energy. This fluid (refrigerant vapor) is then compressed to rise his temperature and pressure. A compressor provides the energy to the system.

In a condenser the fluid is cooled down and transfers his energy to the heating cycle. After the condensation process the working fluid passes through an expansion valve and the pressure gets lower, the process starts again (Dunn, unknown). Image 1 shows the schematic representation of a ground source heat pump.

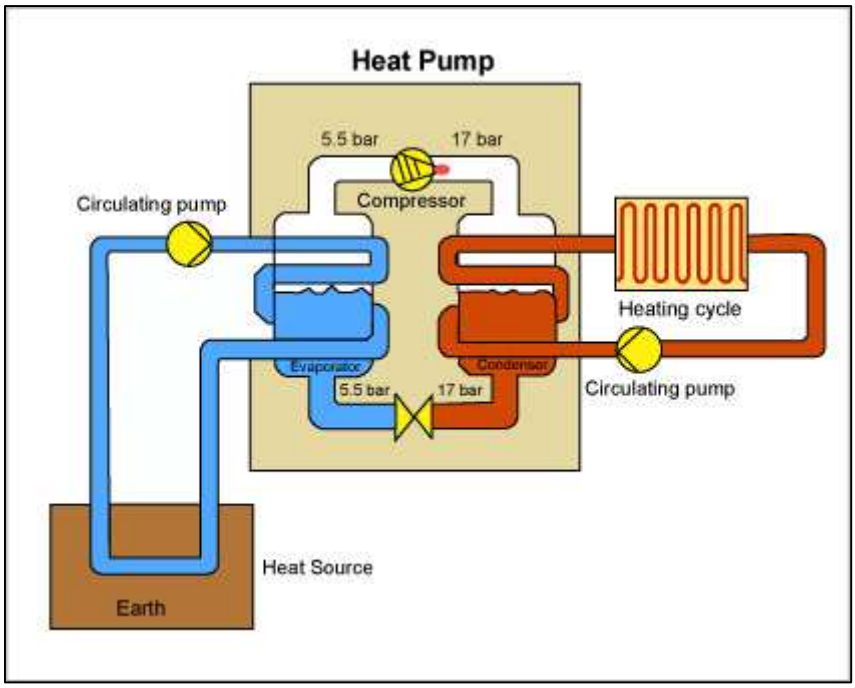

Image 1: Ground sourced heat pump systems (GeoproDesign, 2009)

In Europe, the number of installed Ground Source Heat Pumps was at about 600.000 in the beginning of 2007 with an overall power of approximately 7.329 MW. The country with most GSHP installed is Sweden followed by Germany and France. Considerable numbers of installed GSHP systems also can be found in Austria, Denmark and Finland with over 30.000 each (Conde Lázaro & Ramos Millán, 2009).

The used heat sources can be natural groundwater or collectors installed in the underground in which a fluid circulates. In the first case the natural groundwater is used directly, it is pumped up with a well and transported to the heat exchanger. After extracting energy it is re-injected to the ground. These systems are called Open Loop Systems.

In the second case a fluid circulates through the collectors which are installed in the underground. The fluid is heated up on his way in the collectors and transports the energy to the GSHP system. This type of systems are called Closed Loop Systems (LLOPIS TRILLO & LÓPEZ JIMENO, 2009)

1.1.1. Open Loop System

The simplest case of geothermal energy use is the open loop system. If the access to an aquifer is available and the groundwater quality is sufficiently high, water can be extracted directly from the aquifer. The water is pumped to building and there, energy is extracted by the GSHP system. Normally the used water is re-injected to the aquifer by a second well (injection well).

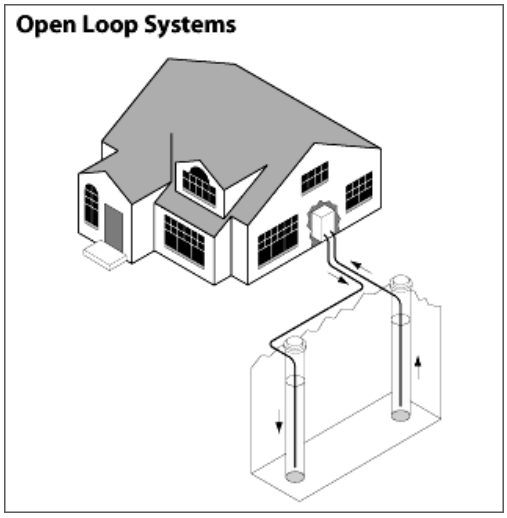

Image 2: Geothermal Heat Pump, Open Loop System (Energy, 2011)

For the operation of an Open Loop System an adequate supply of groundwater must be available. The amount of water required depends on the size of the system to be installed. An inadequate water supply reduces the efficiency and heat transfer capability of the system. Another important factor which has to be considered is the groundwater quality. Important factors are the Calcium and Magnesium content, pH level, Hydrogen content and Chlorine content. Before the installation a water test has to be performed to determine if the quality of the available water meets manufacturer´s requirements. If the water is re-injected to the same aquifer, the distance between extraction and injection well has to be sufficient to avoid interferences between the injected colder water and the extracted warm water (Silberstein, 2003).

Disposal of wastewater

After passing the heat pump or heat exchanger the water has lost part of its heat energy. The groundwater, originally extracted with a temperature of 10℃, may be re -injected with about 5 ℃. There exist several options what to do with the colder “Wastewater” (Banks, 2008):

- Disposal of the wastewater to a surface water body
- Re-injection of the used water to the abstracted aquifer

The re-injection of the wastewater to the same aquifer that it was abstracted from is an attractive solution because it causes no water resources implications. The re-injection of small quantities of water can be realized with a soakaway drainage, larger quantities require the installation of one or more re-injection wells. The injection well should be placed in flow direction to avoid interferences between extraction and injection well.

- Disposal to another aquifer

  If there are several aquifers below the site, the abstracted groundwater can be re-infiltrated or re-injected to another. This helps to avoid interferences between warm and cold water.

- Disposal of wastewater to the abstraction well
  In smaller systems the colder waste groundwater may be re-injected to the upper part of the abstraction well. The cool re-injected water takes a finite time to flow down to the pump and its temperature re-equilibrates on the way down.

Advantages of open loop systems are (ETI-Brandenburg, 2010):

- Only small area is required
- Higher efficiency than closed systems
- Temperature level of the ground water is relatively constant during year (high temperature level)
- Possibility of heating and cooling
- Simple and reliable technique

Disadvantages are:

- Complex and costly construction
- Requires a relatively high groundwater quality

1.1.2. Closed loop systems

If the quality or amount of the available ground water is not sufficient for the installation of an Open Loop System or if local authorities do not allow the extraction of groundwater a Closed Loop System has to be used. In Closed Loop Systems the liquid medium which is used to transport heat from the ground to the heat pump is an antifreeze solution which circulates in a closed loop. The system never gets in direct contact to the aquifer system. The antifreeze solution flows through a piping arrangement and either absorbs heat or transfers heat to earth. The configuration of the pipes depends on the available space and depth that can be reached in the underground (Silberstein, 2003).

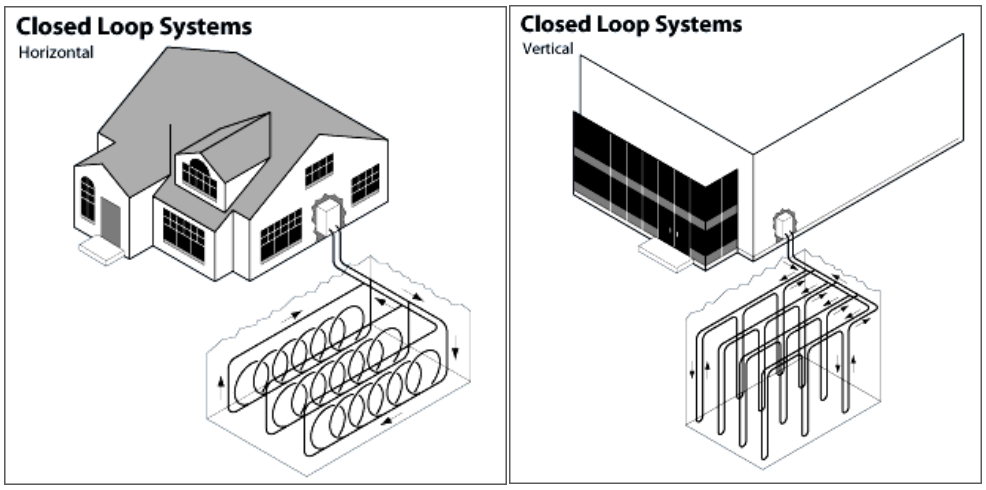

Image 3: Geothermal Heat Pump, Closed Loop System (Energy, 2011)

The ground collector which abstracts heat from the ground can be installed horizontally or vertically. Horizontal collector installations require a relatively big area, installation depth is usually about 0.8 to 1.5 m. Vertical loops have the advantage of small installation area requirements. The costs for a geological report, an eventual test drilling and the installation of the vertical loop by an authorized drilling company are much higher than for horizontal installations (Ochsner, 2007).

Closed loop systems can be of two types: direct circulation and indirect circulation.

In direct schemes, the heat pump´s refrigerant circulates through a tube system which can be a vertical borehole or a horizontal loop. In effect, the subsurface ground loop acts as the evaporator of the heat pump. This system has the disadvantage that the refrigerant of the heat pump circulates directly in the underground. Commonly used refrigerants are fluorocarbons such as R407c which is known as potential groundwater contaminant. In Austria investigations are made to use other substances like CO_2 as refrigerant fluid.

To avoid the direct circulation of the refrigerant fluid in the ground, a carrier fluid can be used to transport the heat from the ground to the heat exchanger. These systems are called Indirect Closed Loop Systems. The carrier fluid is usually a water-based antifreeze solution which allows to operate the system at temperatures below 0 ℃ if necessary. The antifreeze may be a solution of ethylene glycol, ethanol or of salt. These refrigerants a less toxic and biodegradation is much faster (Banks, 2008).

1.2. Heat transport simulation

The increasing number of installed GSHP system leads to the question of how these systems may affect the natural heat distribution in aquifer systems. Changes in groundwater temperatures caused by industrial or domestic thermal use could have influences on other geothermal systems or impacts on the ecological system in the ground. Interferences between geothermal systems lead to a decreasing efficiency and has to be avoided.

Geothermal energy can only be economically competitive as long as applications are designed correctly and adapted to the geological conditions (Armstrong & Blundell, 2007).

The correct design of a geothermal system requires knowledge about the hydro-geological conditions and the temperature distribution in the subsurface. For this reason in the 1970 countries like the USA, France, Sweden and Germany realized field investigations to get a better understanding of heat transport in the subsurface. These methods were effective but due to its complexity very costly. To make reliable and economical predictions of heat distribution and heat plume evaluations, heat transport models had to be developed. The simulated temperature distributions are the bases for the design of the geothermal installations.

Nowadays there exist a great variety of software for heat transport simulation such as SHEMAT and FEFLOW. In this present work MT3DMS, a program developed by Zheng and Wang (Zheng & Wang, 1999), was used for heat transport simulation. The code was originally written for solute transport simulation and was verified for heat transport by Hecht (Mendez Hecht, 2008).

Many investigations on heat transport in the subsurface have been made so far. Most of them were assuming homogenous aquifer conditions. Kupfersberger developed a 2D numerical groundwater model to simulate the impact of groundwater heat pumps on groundwater temperature in the Leibnitzer Feld aquifer, Austria. He validated the simulated results comparing them to field site measurements (Kupfersberger, 2009). A three-dimensional density-dependent groundwater flow and thermal transport model was developed and validated using the results of the thermal injection experiment by Molson (Molson, 1992).

The effect of heterogeneity on heat transport simulation was the object of several investigations over the last few years. Fergusen presented a study on the topic, using stochastic modeling with geostatistics for two aquifers with low and high degrees of heterogeneity. He concluded that there is considerable uncertainty in the distribution of heat associated with injection of warm water into an aquifer (Ferguson, 2007). Bridger and Allen developed a model to evaluate the influence of aquifer heterogeneity, as result of geologic

layering, on heat transport and storage in an aquifer used for thermal energy storage. They used FEFLOW to create a three-dimensional groundwater flow and heat transport model (Bridger & Allen, 2010). All these investigations considered only the heterogeneity of the permeability, porosity and thermal conductivities were assumed to be constant.

Another approach on this topic was made by Shuang Jin. In her work she investigated the effect of heterogeneity of hydraulic and thermal conductivities on the configuration of the temperature plume. She set up several synthetic models with different degrees of logarithmic hydraulic conductivity variances. She concluded that heterogeneity in permeability has a dispersive effect on the temperature plume. In further step she calculated porosity and thermal conductivity and introduced them to the model. She indicated that these parameters seemed to be less important but simulations were incomplete and further investigation had to be done.

1.3. Objectives

This work was made in order to get more information about heat transport modeling in aquifer systems. Based on the results obtained in former works (Shuang, 2009), further investigation on how heterogeneity affects heat transport simulation was made. Synthetic aquifers with different grades of heterogeneity were created using geostatistics (SGeMS). Various heat transport simulations were realized using MT3DMS as heat transport code. To evaluate the importance of heterogeneity in permeability as well as heterogeneity in porosity and thermal conductivity, different simulations with homogeneous and heterogeneous parameters were made and compared to each other.

The primary objects of this work are:

- Analysis of the influence of heterogenic permeability distribution on heat transport simulations in shallow geothermal systems.
- Analysis of the influence of heterogenic permeability, porosity, bulk density and thermal conductivity distributions on heat transport simulations in shallow geothermal systems.
- Heat plume evaluations and application on a test field site.

The mean values of permeability and porosity as well as injection rate and temperature were taken from a field site study. Also the model dimensions and the well layout were chosen considering a report on a field study to link the investigation to a practical application.

2. HEAT AND SOLUTE TRANSPORT IN POROUS MEDIUM

2.1. Hydraulic properties of the subsurface

2.1.1. Hydraulic conductivity (Permeability)

The hydraulic conductivity (Permeability) is a parameter which describes the ability of a geologic material to transmit groundwater. It is a very important parameter in the simulation of groundwater flow and transport. In Darcy`s law the hydraulic conductivity gives proportionality factor k:

$$Q = -kA\frac{\Delta h}{\Delta L}$$

The hydraulic conductivity depends on properties of the solid matrix as well as on properties of the fluid (viscosity, density).

There exist several laboratory and field methods to determinate values for k. A very common approach is the indirect determination of the hydraulic conductivity from grain size analysis. Various investigators found empirical correlations between grain size distribution and hydraulic conductivity (Hazen, 1893), (Krumbein & Monk, 1942). Direct determination methods are steady or quasi-steady flow techniques or a transient flow test (Singhal & Gupta, 1999). Commonly used field methods are the Packer Test, Slug Test and Pumping Tests.

In this work, the hydraulic conductivity of the field side was calibrated with a pumping test. In former investigations on the same field site (Shuang, 2009) the hydraulic conductivity was calculated with empirical formulas using the grain size distribution of the soil. The results are similar to the ones of the pumping test.

Pumping test

In a pumping test (also “aquifer test”), ground water is pumped from an aquifer to get information about important aquifer parameters. The test configuration consists in a production well which pumps groundwater in order to stress the system and one or more observation wells.

The most important parameters measured in a pumping test are the drawdown and the time of drawdown. The drawdown is the decline of the water level measured in the observation wells. It increases with time and pumping rate and decreases with distance from the pumping well (Kasenow, 2001).

Pumping test can be realized with constant or variable pumping rate and the well can penetrate the aquifer fully or partially (Roscoe Moss, 1990).

There exist various solutions for all types of aquifers. The analysis of the drawdown and the calculation of the aquifer parameters is usually made with software packages for aquifer tests like AQTESOLVE.

2.1.2. Porosity

Porosity (or total porosity) is the void volume V_v divided by the total volume (bulk volume) V_t of the porous media.

$$n_t = \frac{V_v}{V_t}$$

It usually expressed in percentages. The total porosity considers the total void volume, regardless of whether pores are connected or not. Due to the fact that water only moves through interconnected pores, another concept of porosity had to be defined for flow simulations. The volume fraction of interconnected pores is called effective porosity (Bear, 1972):

$$n = \frac{V_{vi}}{V_t}$$

Where V_{vi} is the volume of interconnected pores and V_t the total volume (bulk volume) of the medium.

The effective porosity has two important effects on transport simulations. It is used to determine the seepage velocity which controls the advective transport and it affects the pore volume of a model cell available for storage of solute mass (Zheng & Bennet, 2002).

2.1.3. Relationship between porosity and hydraulic conductivity

As discussed before effective porosity and hydraulic conductivity are important parameters in flow and transport simulations in porous media. The hydraulic conductivity is usually determined with aquifer tests such as pumping test or sieve analysis while the porosity is estimated in laboratory test and borehole measurements.

In this work synthetic hydraulic conductivity fields were generated to simulate heterogeneity of the parameters. The idea was to calculate the effective porosity for each cell using the corresponding hydraulic conductivity value.

Over several decades the relationship between porosity and hydraulic conductivity has been object of various studies. The common approach was to calculate hydraulic conductivity from porosity values obtained in field or laboratory tests. In unconsolidated aquifer systems the hydraulic conductivity is usually assumed to be positively correlated with the porosity but the correlation seems to be partial and nonlinear. To achieve reliable correlation models, information about grain size and pore size distribution has to be incorporated (Hu, 2009).

As the required knowledge of size distribution and spatial arrangement of the pore channels is not always available it´s difficult to determine an appropriate relationship between permeability and porosity. The most common approach to relate permeability with porosity is the model of Kozeny and Carman (Carman, 1937) (Kozeny, 1927). This model provides a link between media properties and flow resistance in the pore channels (Costa, 2005).

The idea of Kozeny and Carman was to relate permeability with porosity and grain size. In their first approach they presented following equation (Dvorkin, 2009):

$$k \sim d^3 \cdot n^3$$

They modified their equation introducing constants and about half a century ago Kozeny and Carman presented the following semiempirical, semitheoretical formula to predict permeability.

$$k = \left(\frac{\gamma}{\mu}\right) \cdot \left(\frac{1}{C_{C-K}}\right) \cdot \left(\frac{1}{S_0{}^2}\right)\left(\frac{e^3}{1+e}\right)$$

Where γ is the unit weight of the fluid, μ the viscosity of the fluid, $C_{C\text{-}K}$ the Kozeny-Carman empirical coefficient, S_0 the specific surface area per unit volume of particles [1/cm] and *e* the void ratio. Carman suggested in 1956 a value of 4.8±0.3 for the Kozeny-Carman coefficient $C_{C\text{-}K}$. Introducing unit weight and viscosity of water the Kozeny-Carman equation has the following form (Carrier, 2003).

$$k = 1.99 \cdot 10^4 \cdot \left(\frac{1}{S_0{}^2}\right)\left(\frac{e^3}{1+e}\right)$$

The specific surface area S_0 can be calculated from the grain size distribution.

Many researchers have studied the Konzeny-Carman equation and various correlation laws have been found (Mohnke, 2008) (Regalado & Carpena, 2004). All of them have the same limitations as they do not consider extreme particle shape, extreme particle size distribution and anisotropy, etc. (Carrier, 2003) However, this model needs a lot of additional information and is difficult to handle so it´s use for practical application is restricted.

Another approach for the development of a permeability-porosity correlation was presented in 2003 by Schneider. He suggested the following expressions (Schneider, 2003):

$$\log(k) = a + b \cdot n$$

$$n = a' + b' \cdot \log(\mathrm{k})$$

Where k is the permeability and φ the porosity fraction; a, and b are constants which have to be developed from regression of data. The combination of these two trend lines calculated before leads to a representative curve is to find a line halfway between the two previously calculated trends. The final trend line will be defined as the following relationship:

$$\log(k) = a_p + b_p \cdot n$$

Where K is the permeability and n the porosity; a_p and b_p are constants developed from combination of two previous curve fits.

Various investigations realized in the last decades have suggested similar relationships like the one of Schneider. In 1968, Morotz developed an empirical formula which has been cited by many researchers (Matthess & Ubell, 2003) (Shuang, 2009). Another empirical relationship was developed based on field data of Horckheimer Insel site which is located in Neckar valley, Germany.

In 1993, Busch and Luckner presented the following relationship between porosity and permeability where the coefficients were determined empirically (Busch & Luckner, 1993):

$$n = 0.05 \cdot logk + 0.4$$

In this work the porosity values where calculated from the generated permeability fields using the presented formula of Busch and Luckner. One reason to choose this relationship was the simple linear relationship with few parameters which avoids further errors due to introduction of empirical parameters. The other reason was that the obtained results were the closest to the mean value of the field site.

2.1.4. Dispersivity coefficient

Transport simulations in aquifer systems are driven by various processes. One of them is called the hydrodynamic dispersion. Hydrodynamic dispersion describes two transport mechanisms: Mechanical dispersion and Molecular diffusion. Mechanical dispersion is a phenomenon caused by differences in the flow velocity. An initial cloud of a contaminant is spread out due to differences in flow velocity and direction. The Molecular diffusion of a contaminant in a fluid is caused by the random motion of the molecules (Brownian motion). It causes an additional flux of the components particles from regions of higher concentrations to regions with lower ones. As these two processes occur simultaneously it is almost impossible to separate them and the term Hydrodynamic dispersion includes both of them (Bear & Cheng, 2010).

The dispersive flux is usually described by laws similar to Fick´s law for molecular diffusion (Zheng & Bennet, 2002).

$$J = -D\frac{\partial C}{\partial x}$$

where J is the flux vector, D the dispersion coefficient and $\frac{\partial C}{\partial x}$ the concentration gradient. This leads to following expression (Anderson & Woessner, 1992):

$$\frac{\partial c}{\partial t} = \frac{\partial}{\partial x_i}\left(D_{ij}\frac{\partial c}{\partial x_j}\right)$$

D_{ij} is the dispersion coefficient which can be described as follows:

$$D_{ij} = a_{ijmn}\left(\frac{v_m v_n}{v}\right) + D_m$$

D_m is the coefficient of molecular diffusion, α_{ijmn} are called the dispersivity coefficients (Anderson & Woessner, 1992).

In an isotropic porous medium the component of the dispersivity reduces to two. They are called longitudinal and transverse dispersivities and the denotations are α_L and α_T. The transverse dispersivity is divided into horizontal transverse and vertical transverse dipersivity. The longitudinal dispersivity represents the local variations in the velocity field of a groundwater solute parallel to the fluid flow direction, the transverse dispersivities the variation perpendicular to the flow direction.

There exist numerous studies which try to characterize dispersivity values for field-scale application. The obtained values generally appear to be dependent on the scale of observation. Most of the recent field-scale tests clearly indicate a trend of increasing longitudinal dispersivity with increasing scale of observation (Bear & Cheng, 2010).

Image 4 shows a plot of longitudinal dispersivity values for unconsolidated media obtained from laboratory tests, aquifer tests and computer model vs. the corresponding scale of measurement. The plot shows that longitudinal dispersivity increases exponentially with the scale of measurement.

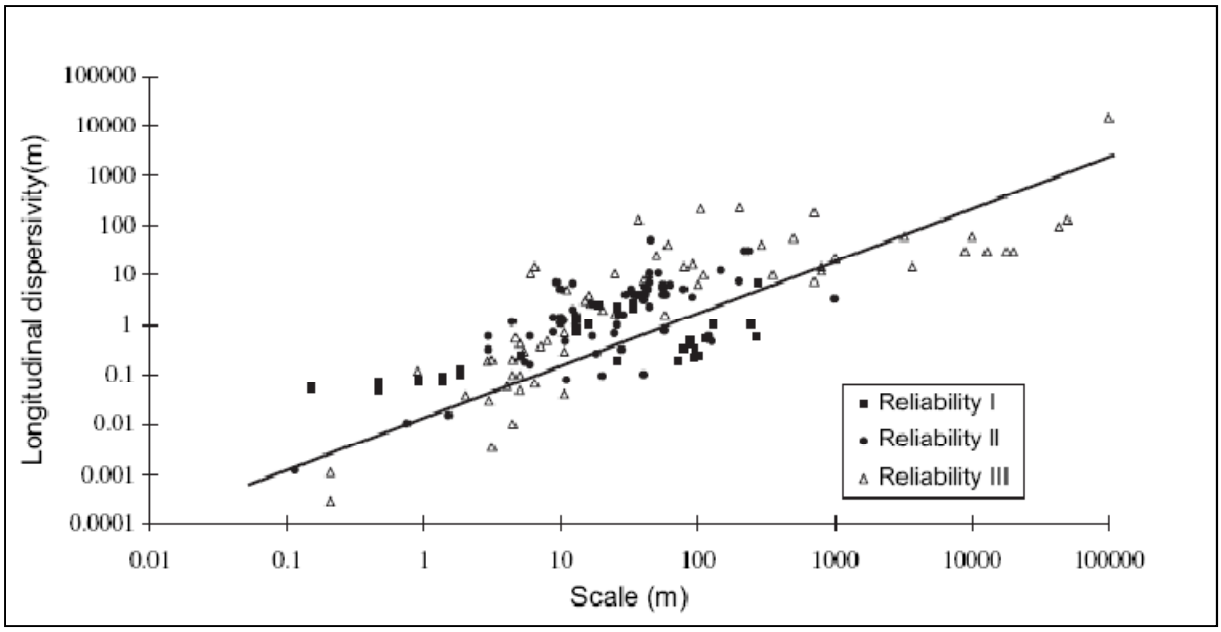

Image 4: Relationship of longitudinal dispersivity to scale of measurement for unconsolidated sediments (Schulze-Makuch, 2005)

There are certain doubts if dispersivities for solute transport and heat transport are comparable. The fact that heat, in contrary to solutes, is transported not only through the liquid phase but also through the solid phase indicates that there could be differences in dispersivity coefficients for heat and solute transport.

However in this work, solute and heat transport dispersivities are assumed to be comparable. The values for longitudinal dispersivity were estimated using the Plot of Image 4.

2.2. Thermal properties of the subsurface

2.2.1. Thermal conductivity

The thermal conductivity λ is the ability of a solid or fluid to conduct thermal energy in form of heat. It has the dimension [$W/m^{-1}K^{-1}$].

An aquifer system is a multiphase medium and for this reason the thermal conductivity of the solid and of the fluid phase has to be considered. This can be realized by the introduction of an overall thermal conductivity. It depends mainly on the geometry of the medium and the grade of saturation. Table 1 gives typical values for λ:

Table 1: Thermal conductivity of different material (Jessberger & Jagow-Klaff, 2001)

Type of soil	Thermal conductivity λ [$W/m^{-1}K^{-1}$]
Gravel	2.0-3.3
Sand	1.5-2.5
Silt	1.4-2.0
Clay	0.9-1.8
Claystone	2.6-3.1
Sandstone	3.1-4.3

There are different methods to calculate the overall thermal conductivity of a porous medium considering the conductivities of the fluid (λ_f) and solid (λ_s) phase (Nield & Bejan, 1999).

If the heat conduction is assumed to occur mainly in parallel the overall thermal conductivity λ_e can be calculated using the weighted arithmetic mean of λ_f and λ_s.

$$\lambda_{ari} = (1 - n) \cdot \lambda_s + n \cdot \lambda_f$$

If heat conduction takes place mainly in series the overall conductivity is the weighted harmonic mean of λ_f and λ_s.

$$\lambda_{har} = \frac{(1 - n)}{\lambda_s} + \frac{n}{\lambda_f}$$

For practical purposes the geometric mean of λ_f and λ_s gives a good estimate as long as λ_f and λ_s are not too far from each other (Nield & Bejan, 1999):

$$\lambda_{geo} = {\lambda_s}^{(1-n)} + {\lambda_f}^{n}$$

The geometric mean equation shows a good match with the experimental data for unconsolidated and consolidated material. For unconsolidated material the V`ries equation matches even better (Shuang, 2009).

In the present work the geometric mean formula was applied to calculate the thermal conductivity of the saturated porous medium.

2.2.2. Specific heat capacity

The specific heat capacity is defined as the quantity of heat required to change one unit mass of a sustance by one degree in temperature. The specific heat capacity c is related to one unit mass of the substance.

$$c = \left[\frac{J}{kg \cdot K}\right]$$

Table 2 gives typical values for the Specific heat capacity of different materials:

Table 2: Specific heat capacities of different substances (www.engineeringtoolbox.com) and * (Molina Giraldo, 2008)

Material	Specific heat capacity c [$Jkg^{-1}k^{-1}$]	Density ρ [$kg\ m^{-3}$]
Water	4187	1000
Basalt rock	840	2400-3100
Clay	920	1800-2600
Limestone	840	2700-2800
Quartz sand	830	2650
Sandstone	896*	2375 *

If the heat capacity is given per unit volume of a substance, it is called the volumetric heat capacity ρc. It can be calculated multiplying c by the density ρ.

$$\rho c = \left[\frac{J}{m^3 K}\right]$$

For a porous medium an effective volumetric heat capacity has to be defined considering the solid and the liquid phase (Corapcioglu, 1996):

$$(\rho c)_e = n \cdot \rho_f c_f + \rho_b c_s$$

Where $(\rho c)_e$ is the effective volumetric heat capacity, $\rho_f c_f$ the volumetric heat capacity of the fluid and $\rho_s c_s$ the volumetric heat capacity of the solid.

The heat capacity of a soil is influenced by temperature, pressure, porosity and grade of saturation.

2.3. Governing equations

2.3.1. Solute transport in a porous saturated media

Solute transport in a porous medium is mainly driven by two physical phenomena: Advection and Hydrodynamic Dispersion. Transport by advection describes the movement of the solute caused by the flowing fluid. Hydrodynamic dispersion is a transport process caused by local heterogeneities and concentration gradients (Kulasiri & Verwoerd, 1992). For a full description of transport and evolution of a solute in a porous saturated media it is also necessary to consider Chemical reactions and Sources/Sinks.

Transport by Advection

The process called advection considers the movement of the solute with the average seepage velocity of the groundwater flow. If we consider only advective transport we take the assumption that all particles move with the same velocity. Equations of this type are called Advective Transport Equations (Zheng & Bennet, 2002). This assumption is only valid if flow velocities are high, for low flow velocities the process of dispersion has to be incorporated in the model.

Transport by Dispersion

The term hydrodynamic dispersion describes two transport processes:

- Mechanic dispersion
- Molecular diffusion

Mechanic dispersion is a transport process caused by fact that not all particles move at the same average velocity. Local heterogeneities cause differences in the moving velocities of the particles. The movement of solute particles caused by concentration gradients is called molecular diffusion.

Like discussed before, the dispersive flux is usually described by laws similar to Fick´s law for molecular diffusion.

$$n \cdot \frac{\partial C}{\partial t} = \nabla[n(D_m + \alpha_s v_a)\nabla C]$$

This expression consider the two processes simultaneously D_m is the molecular diffusion coefficient and α_s the dispersivity coefficient.

Sources and sinks

The sources and sinks term considers all possible injections or extraction of solute to or from the aquifer. It represents the change of mass per unit of time and volume in the system.

Chemical processes

Typical chemical reactions implemented in transport models are adsorption and hydrolysis or decay. Adsorption is described by a retardation factor R

$$R = 1 + \frac{\rho_b \cdot K_d}{\theta}$$

The retardation factor is a simplified concept to describe the relationship between the total concentration of contaminant (liquid and solid phase) and the mobile solute in the liquid phase. ρ_b is the bulk density [kg/m^3] and K_d the distribution coefficient.

Hydrolysis and decay are usually described by a first order rate constant

$$\frac{dC}{dt} = r \cdot C$$

The concept of the first order decay is pretty simple and only adequate to describe simple contaminant problems.

Solute transport with MT3DMS

Writing a mass balance the advection-dispersion equation for solute transport can be obtained. The partial differential equation for solute transport in transient groundwater flow which is used by MT3DMS has the form (Zheng & Wang, 1999):

$$n \cdot \frac{\partial C}{\partial t} + \frac{\rho_b K_d}{n} \cdot \frac{\partial C}{\partial t} = \nabla[n(D_m + \alpha_s v_a)\nabla C] - \nabla(v_a n C) + q_s C_s - rnC$$

n	*Porosity*	-
C	*Disolved mass concentration*	$kg\ m^{-3}$
ρ_b	*Bulk density*	$kg\ m^{-3}$
K_d	*Distribution coefficient*	$m^3 kg^{-1}$
D_m	*Coefficient of molecular diffusion*	$m^2\ s^{-1}$
α_s	*Dispersivity coefficient*	m
v_s	*Flow Velocity*	$m\ s^{-1}$
q_s	*Flow rate of sources and sinks*	$m^3 s^{-1}\ m^{-3}$
C_s	*Concentration sources and sinks*	$kg\ m^{-3}$
r	*Reaction rate constant for the dissolved phase*	s^{-1}

The left hand side of the equation represents the transient term with the retardation factor. On the right hand side the term $\nabla(v_a\ nC)$ represents the transport by advection. MT3DMS calculates the velocity field from the hydraulic head distribution, which requires a former calculation by a groundwater flow model (In this work MODFLOW). The term $q_s C_s$ represents the sources and sinks.

2.3.2. Heat transfer in a porous saturated media

The heat transfer in a porous saturated media is mainly driven by two processes, Conduction and Convection.

Conductive heat transfer

Conduction is the transfer of thermal energy caused by a temperature gradient. The law of Fourier describes the heat flux J_H which is the energy flowing through a surface.

$$J_H = -\lambda \frac{\partial T}{\partial x}$$

J_H	*heat flux*	Wm^{-2}
λ	*Thermal conductivity*	$Wm^{-1}K^{-1}$

Conduction takes place through both the solid material and the fluid. According to the second law of thermodynamics the heat flow goes from regions with higher temperatures to regions with lower temperatures (Jiji, 2009).

Convective heat transfer

Convection is the transfer of thermal energy from one place to another, caused by the movement of the fluid. Convection is based on the physical principle called bulk fluid motion (Nield & Bejan, 1999).

Energy equation in a porous medium

The energy equation for the fluid phase can be written as (Nield & Bejan, 1999):

$$\rho_f c_f \cdot \frac{\partial T_f}{\partial t} = \nabla(\lambda_f \nabla T_f) + \nabla(\alpha_h v_a \nabla T_f) - \nabla\left(\rho_f c_f v_a T_f\right) + q_h$$

where λ_f is the thermal conductivity of the fluid, α_h the heat dispersivity coefficient and q_h the source and sink term. The energy equation of the solid phase can be written as follows:

$$\rho_s s \cdot \frac{\partial T_s}{\partial t} = \nabla(\lambda_s \nabla T_s) + q_h$$

Combining the two equations and introducing the porosity relations the partial differential equation for heat transfer considering convection and conduction may be expressed as (Corapcioglu, 1996):

$$n \cdot \rho_f c_f \cdot \frac{\partial T_f}{\partial t} + (1-n)\rho_s c_s \cdot \frac{\partial T_s}{\partial t} = \nabla[(\lambda_e + n \cdot \rho_f c_f \cdot \alpha_h v_a)\nabla T_f] - \nabla(n \cdot \rho_f c_f v_a T_f) + q_h$$

n	*Porosity*	-
T_f	*Temperature of the water*	K
ρ_f	*Density of water*	$kg\ m^{-3}$
c_f	*Specific heat capacity of water*	$W\ s\ kg^{-1}\ K^{-1}$
ρ_s	*Density of the solid*	$kg\ m^{-3}$
c_s	*Specific heat capacity of the solid*	$W\ s\ kg^{-1}\ K^{-1}$
T_s	*Temperature of the solid*	K
α_h	*heat dispersivity coefficient*	m
q_h	*Heat injection or extraction*	Wm^{-3}
λ_e	*Thermal conductivity*	$Wm^{-1}K^{-1}$
v_a	*Flow velocity*	ms^{-1}

The thermal conductivities of the solid and fluid phase are introduced by the concept of an effective thermal conductivity λ_e.

The left hand side of the equation shows the transient term. Assuming a local thermal equilibrium, $T=T_s$, and defining effective volumetric heat capacity

$$(\rho c)_e = n \cdot \rho_f c_f + (1-n)\rho_s c_s$$

the energy equation may be written as:

$$(\rho c)_e \cdot \frac{\partial T}{\partial t} = \nabla[(\lambda_e + n \cdot \rho_f c_f \cdot \alpha_h v_a)\nabla T] - \nabla(n \cdot \rho_f c_f v_a T) + q_h$$

Heat exchange with the environment can be introduced with the term (Molina Giraldo, 2008):

$$\frac{\lambda_u}{HF}\Delta T'$$

λ_u	*Thermal conductivity of the unsaturated soil*	$Wm^{-1}K^{-1}$
$\Delta T'$	$T\text{-}T_{Environment}$	K
H	*Thickness of the aquifer*	m
F	*Depth of the water table*	m

Introducing equation the heat exchange term and rearranging the other terms the energy equation becomes

$$\left(\frac{(\rho c)_e}{n\cdot\rho_f c_f}\right)n\frac{\partial T}{\partial t} = \nabla\left[\left(\frac{\lambda_e}{n\cdot\rho_f c_f}+\alpha_h v_a\right)\nabla T\right] - \nabla(n\cdot v_a T) + \frac{q_h}{\rho_f c_f} - \frac{\lambda_u}{\rho_f c_f HF}\Delta T'$$

2.3.3. Heat transport modeling with MT3DMS

Like it was mentioned before, the MT3DMS code was originally written to simulate solute transport. The analysis of the heat and solute transport analysis equation shows the similarities of the two processes and with some adaptations MT3DMS can be used for the simulation of heat transport.

$$\left(1+\frac{\rho_b K_d}{n}\right)n\frac{\partial C}{\partial t} = \nabla[n(D_m+\alpha_s v_a)\nabla C] - \nabla(v_a nC) + q_s C_s - \lambda nC$$

$$\left(\frac{(\rho c)_e}{n\cdot\rho_f c_f}\right)n\frac{\partial T}{\partial t} = \nabla\left[\left(\frac{\lambda_e}{n\cdot\rho_f c_f}+\alpha_h v_a\right)\nabla T\right] - \nabla(n\cdot v_a T) + \frac{q_h}{\rho_f c_f} - \frac{\lambda_u}{\rho_f c_f HF}\Delta T'$$

Like discussed before, MT3DMS was verified for heat transport by Hecht (Mendez Hecht, 2008). Comparing the two equations, for each term in the solute transport equation we can obtain a corresponding term in the heat equation.

Chemical reactions

$$\left(1 + \frac{\rho_b K_d}{n}\right) = \left(\frac{(\rho c)_e}{n \cdot \rho_f c_f}\right)$$

The heat exchange between solid and liquid phase is implemented in MT3DMS in the chemical reactions package. The type of sorption has to be set to *linear isotherm sorption*. The input parameters required by MT3DMS to calculate the retardation factor are the *bulk density* ρ_b and the *distribution coefficient* K_d.

Dispersion

$$n(D_m + \alpha_s v_a) = \left(\frac{\lambda_e}{n \cdot \rho_f c_f} + \alpha_h v_a\right)$$

The conductive heat transport is implemented in MT3DMS in the *dispersion package*. The molecular *diffusion coefficient* D_m for heat conduction has to be calculated, the *dispersivity coefficient* α_h can be introduced without adaptations.

Advection

To simulate convective heat transport the *advection package* of MT3DMS has to be activated. MT3DMS provides different solution schemes for the advection term. In this study, simulations using different solution schemes were made. The results and the simulation time where compared to evaluate the most efficient solution method. The most satisfying results were made with the *Hybrid MOC/MMOC (HMOC)* solution scheme.

Sources and sinks

The *sources and sinks* term is introduced in the *well package* of ModFlow and MT3DMS. The temperature *[K]* is treated like a concentration [kg/m^3] the recharge rate is constant *[kg/m^3]*

$$\frac{q_h}{\rho_f c_f}\left[\frac{K}{s}\right] = q_s C_s \left[\frac{kg}{m^3 s}\right]$$

The heat exchange with the environment was assumed to be negligible so no first order reaction was simulated.

Further information about the heat transport with MT3DMS can be found in other studies (Mendez Hecht, 2008)(Molina 2009).

3. MODEL SETUP AND INPUT PARAMETERS

3.1. The field site

In the late 1970´s investigators in Germany made first studies and field experiments to understand the processes of heat transport in shallow geothermal systems. In north Germany the Brenner Consultancy realized investigations on 2 test field sites which are called Esseling site and Egging site. In this work the model dimensions and simulation parameters were chosen considering the results obtained from Esseling site. The information is based on field site descriptions given in former works on this topic (Rasouli, 2008) (Shuang, 2009). The original reports made by Balke and Brenner include the hydrogeologic description of the field, temperature measurements of groundwater, daily air temperature measurements and daily humidity measurements as well as the pumping test measurements and the amount of injected water (Balke & Brenner, 1980).

Geology: The sediments are made of unconsolidated quaternary valley sand belonging to late Pleistocene. The investigation of the aquifer was realized with geoelectric sounding, 2 drilling boreholes, 10 sieve analysis and 20 groundwater observation wells. The aquifer consists of fine middle sand and was investigated in the upper 30 m (Rasouli, 2008) (Balke & Brenner, 1980).

Hydrogeology: The measured groundwater table was varying between 0.4 [m] to 1.5 [m] below the ground due to the seasonal rainfall. The average flow velocity before pumping was about 0.2 [md^{-1}] towards west although there are doubts about the real flow direction. The report of Balke and Brenner also provides values for permeability and effective porosity. Results obtained with sieve analysis give a value 1.04×10-5 [ms^{-1}] for hydraulic conductivity and 2.6 [%] for effective porosity. The pumping test gave 8.25×10-5 [ms^{-1}] for hydraulic conductivity and 3.9 [%] for effective porosity which is more or less the same order of magnitude. The estimated effective porosity seems to be very low and further consideration on this parameter is needed (Shuang, 2009) (Balke & Brenner, 1980).

Equipments: The installed equipment consists of an injection well, groundwater observation wells and a meteorological station. The injection well is about 16.4 m deep and has a diameter 150 mm. The well is partially penetrating with a filter placed from 8.8 m to 14.8 m.

Water Injection: The injection started at 15th of August 1978 and ended on 15th of June 1979. The total time of injection was 304 days due to a vacation period were no water was injected. The injected water had a temperature range between 4 and 7.8 ℃ with an average of 5 ℃. The maximum pumping rate was 42 m^3d^{-1}. (Rasouli, 2008)

Table 3: Hydraulic and thermal properties of the Esseling field site

Parameter	Symbol	Value	Unit
Aquifer thickness	H	33	[m]
Density of the solids	ρ_s	0.36	[kgm^{-3}]
Hydraulic conductivity	k	$8.25*10^{-5}$	[md^{-1}]
Total porosity	n_t	0.36	[-]
Effective porosity	n	0.039	[-]
Hydraulic gradient	i	$1.15*10^{-3}$	[-]
Seepage velocity	v_a	$5.9*10^{-5}$	[ms^{-1}]
Specific heat capacity of the soil	c_s	840	[$Jkg^{-1}K^{-1}$]
Specific heat capacity of the water	c_w	4190	[$Jkg^{-1}K^{-1}$]
Overall thermal conductivity	λ_e	2.85	[$Wm^{-1}K^{-1}$]
Initial groundwater temperature	T_0	10.19	[K]
Mean temperature of the injected water	T_{in}	4.58	[K]
Mean water injection rate	Q	15.76	[m^3d^{-1}]
Total time of injection	t	304	d

3.1.1. Well configuration

Image 5 shows the test field configuration of Esseling site and the initial hydraulic heads. The well Br was used for the injection of the cold water and for water extraction in the pumping test. The other 8 wells were used to make the observations in the saturated zone up to 20 m of depth. Wells nr. 3, 4, 5, 6 have a distance of 5 m to the injection well Br, nr. 7, 9, 11, 13 are located at 13 m. The well Z is the reference point which is located at 57 m from the injection well (Rasouli, 2008).

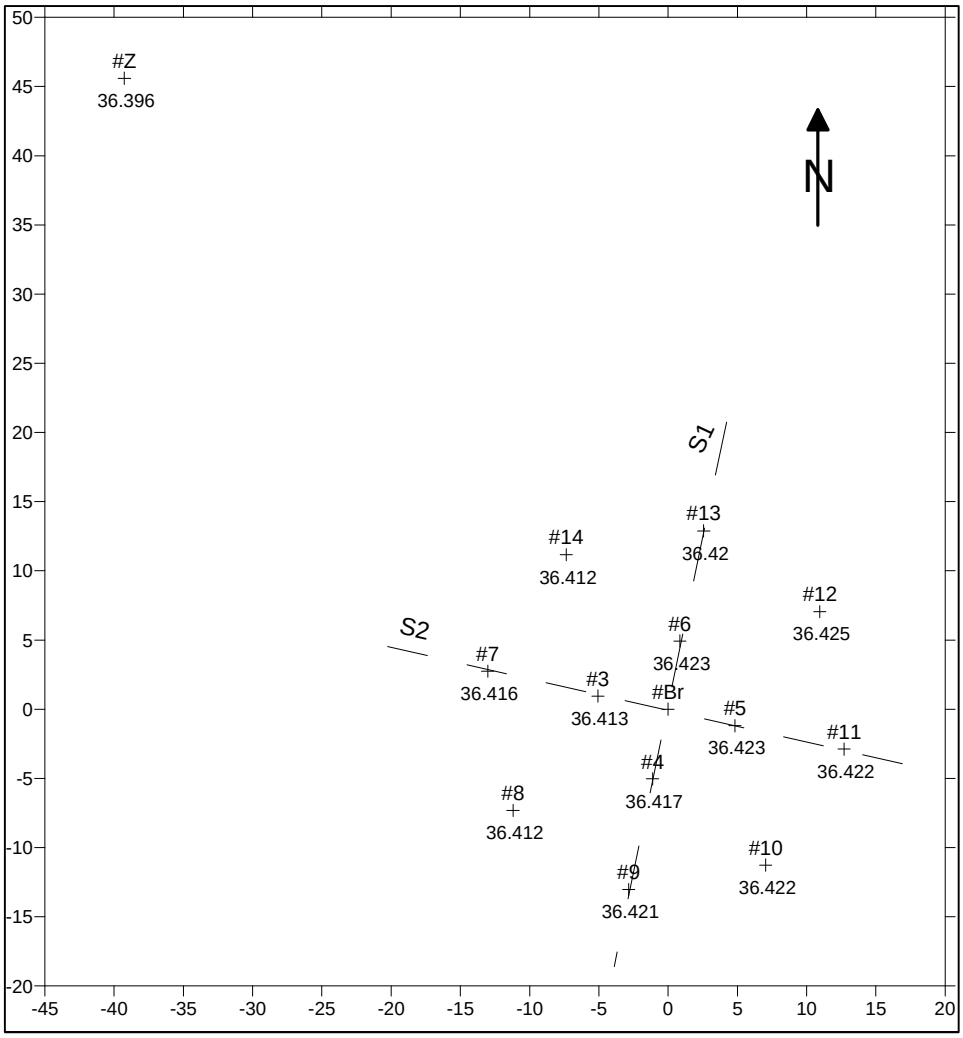

Image 5: Well configuration and initial hydraulic heads of Esseling site (Shuang, 2009)

Due to the shallow gradient certain problems occurred in the determination of the flow direction. The real flow direction could not be determined due to lack of measurements. Observing the initial hydraulic heads the flow direction seems to be towards west/north-west. The hydrogeology map of the area indicates a flow direction to the north (Shuang, 2009).

Because of the uncertainty about real flow direction and hydraulic gradient these value were assumed for the simulations made in this work.

3.1.2. Pumping Test

To calibrate the hydraulic properties of the field site a reconstruction of the 2 phase pumping test of Esslingen site was realized. The drawdown results given in the report of Balke and Brenner were used to reconstruct the interpretation of the pumping test results (Balke & Brenner, 1980). Pumping started at 11.36 on March 3 1978 with a pumping rate of 5.2 [m^3h^{-1}]. On March 5 at 11.25 the pumping rate was augmented to 11.9 [m^3h^{-1}].

The well Br was used as a pumping well to extract water from the aquifer. The other wells were used for observation of the hydraulic head drawdown. Table 4 shows the 2 pumping rates and the time of pumping (Balke & Brenner, 1980) (Shuang, 2009).

Table 4: Pumping data for AQTEsolv

Time after pumping started [h]	Pumping rate [m^3h^{-1}]
2.26	5.2
4.40	5.2
7.06	5.2
11.65	5.2
23.31	5.2
25.83	5.2
30.56	5.2
47.48	5.2
58.91	11.9
67.4	11.9
81.95	11.9
105.48	11.9

The calculation of the hydraulic conductivities was made in a test version of AQTESOLVE, downloadable on the Homepage. Input parameters are the pumping data of Table 4 and the observed drawdown in each of the observation wells given in the report of the test field site. In the report provides the hydraulic head the observation well after each pumping period.

AQUTESOLVE provides various solution methods for different types of aquifers (AQTESOLVE, 2011). For this work the Neuman solution for unconfined aquifers and partially penetrating pumping and observation wells was chosen to calculate transmissivities. It provides solutions for variable pumping rates as well as for multiple pumping and observation wells (Neuman, 1974)

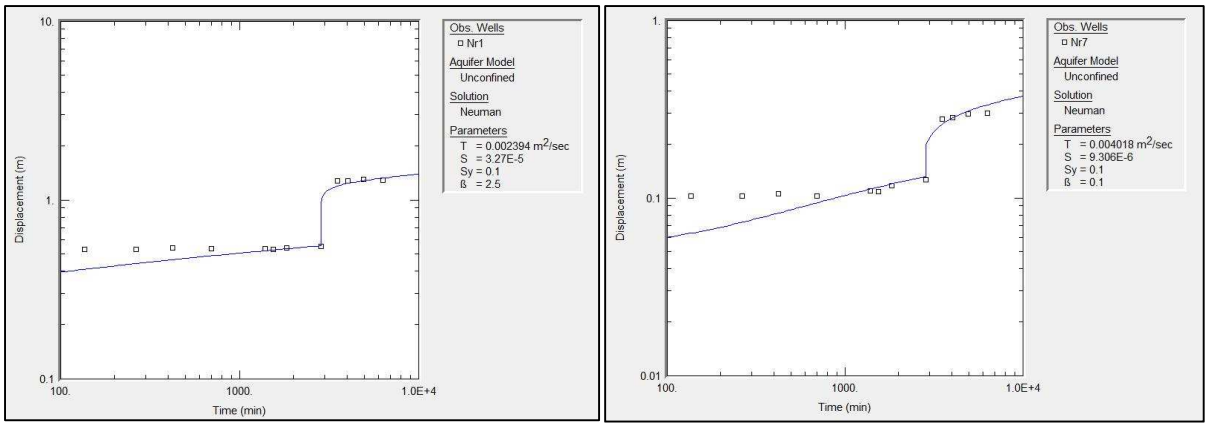

Image 6: Solutions of AQTEsolv for well Nr.1 and well Nr.7

Image 6 shows the adjusted drawdown curves and the calculated transmissivities of well Nr. 1 and 7 obtained applying Neumans solution. The transmissivities obtained with AQTESolve and the calculated logarithmic hydraulic conductivities of all wells are given in Table 5. Hydraulic conductivities were calculated from the transmissivities.

Table 5: Results of the pumping test

Well	**T_{ab} [m^2s^{-1}]**	**K_{ab} [ms^{-1}]**	**log K_{ab}**
1	2.39E-03	7.25E-05	-4.14
2	4.14E-03	1.25E-04	-3.90
3	5.27E-03	1.60E-04	-3.80
4	5.39E-03	1.63E-04	-3.79
5	5.28E-03	1.60E-04	-3.80
6	5.68E-03	1.72E-04	-3.76
7	4.02E-03	1.22E-04	-3.91
8	4.38E-03	1.33E-04	-3.88
9	4.83E-03	1.46E-04	-3.83
10	4.64E-03	1.41E-04	-3.85
11	4.64E-03	1.41E-04	-3.85
12	5.01E-03	1.52E-04	-3.82
13	4.47E-03	1.35E-04	-3.87
14	4.34E-03	1.31E-04	-3.88
Z	5.57E-03	1.69E-04	-3.77
Mean	4.67E-03	1.41E-04	**3.86E+00**
Standard deviation	7.89E-04	2.39E-05	**8.80E-02**

The mean value and the standard deviation of the pumping test results are close to the values which were obtained in former studies (Shuan Jin 2009).

3.2. The Model layout

The model layout and model dimensions were assumed considering the field site data of Esseling site. It consists in a grid with 100x100 cells and 40 layers. The cell size is 1x1 [*m*] and the layer thickness is 1 [*m*]. The model layout was already used in a former study, the same layout was chosen to compare results (Shuang, 2009). Because of the problems in the characterization of the upper 10 m of an unconfined aquifer, the aquifer is assumed to be confined (Rasouli, 2008).

The left and the right boundary of the model are assigned constant head boundaries *(ibound -1).* The upper and lower boundary and the bottom of the model are no-flow boundaries. All other cells are assigned active flow cells *(ibound 1).*

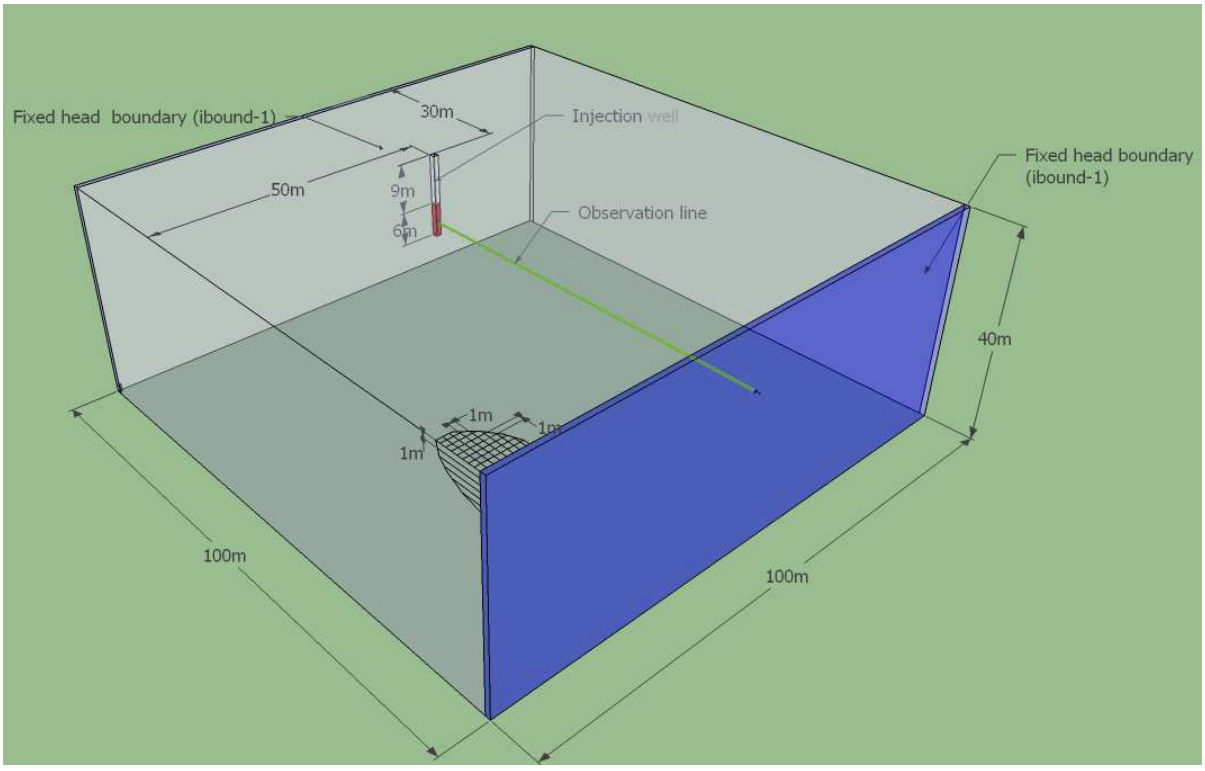

Image 7: Aquifer Model of Esseling site

In this study the simulations were made assuming a hydraulic gradient of *i=0.02*. The assigned constant heads are 45 [m] on the left hand boundary and 43 [m] on the right boundary. Because of the problems in the determination of the flow direction and the

hydraulic gradient explained in chapter 3.1, the hydraulic gradient and the constant heads were assumed. The horizontal and the vertical hydraulic conductivities were set equal to make the aquifer isotropic.

The injection well is located in cell 30, 50 from layer 10 to layer 15 (Esseling site), the total injection rate was divided and assigned to each layer. The recharge was assumed to be constant over 360 days. The total simulation time was divided into 12 stress periods and a steady state simulation was performed.

3.2.1. Input Parameters for Modflow

Table 6: Input parameters for Modflow

Parameter	Symbol	Value	Unit	Reference
Layer type		0: confined		(Rasouli, 2008)
Time	t	3.11E+7	s	assumed
Horizontal hydraulic conductivity	K_x	0.00014	ms^{-1}	(Esseling site)
Vertical hydraulic conductivity	K_z	0.00014	ms^{-1}	(Esseling site)
Effective porosity	n	0.26		assumed
Total recharge rate	Q	1.84E-4	m^3s^{-1}	(Esseling site)
Pumping rate Wells (layer 10 to 15)		3.05E-5	m^3s^{-1}	calculated

3.2.2. Input Parameters MT3DMS

MT3DMS requires the definition of the concentration boundary conditions. A constant concentration boundary *(icbound -1)* was assigned to the left hand boundary of the model, all other cells are active concentration cells *(icbound 1).*

The advection term of the transport equation was solved with the *Hybrid MOC/MMOC (HMOC)* solution scheme because it runs faster than the *Ultimate TVD scheme* and it is free of numerical dispersion (Zheng & Wang, 1999).

The type of sorption in the chemical reaction package is set to *linear isotherm sorption*, no first order reaction was simulated.

Table 7: Input Parameters for MT3DMS

Parameter	Symbol	Value	Unit	Reference
Initial concentration (Inicial temperature)	T_o	283.15	*K*	(Esseling site)
Longitudinal dispersivity	α_L	0.5	*m*	(Schulze-Makuch, 2005)
Horizontal transverse dispersivity	α_h	0.05	*m*	$\alpha_l/10$
Vertical transverse dispersivity	α_v	0.05	*m*	$\alpha_l/10$
Effective molecular diffusion coefficient	D_m	1.838E-6	m^2s^{-1}	(Molina Giraldo, 2008)
Bulk density	ρ_b	1961	kgm^{-3}	calculated
Distribution coefficient	K_d	1.983E-4	m^3kg^{-1}	(Molina Giraldo, 2008)
Concentration well (Temperature)	T_{in}	278.15	*K*	(Esseling site)
Retardation factor	R	2.5		calculated
Density of the solid	ρ_s	2.65	kgm^{-3}	(engineeringtoolbox, Specific-heat-capacity)
Specific heat capacity of solids	c_s	830	$Jkg^{-1}K^{-1}$	(engineeringtoolbox)
Volumetric heat capacity of the solid	$\rho_s c_s$	2200000	$Jm^{-3}K^{-1}$	calculated
Volumetric heat capacity water	$\rho_f c_f$	4185000	$Jm^{-3}K^{-1}$	(engineeringtoolbox)
Volumetric heat capacity of the saturated aquifer	$\rho_e c_e$	2716000	$Jm^{-3}K^{-1}$	calculated
Thermal conductivity of solids	λ_s	3	$Wm^{-1}K^{-1}$	(Jessberger & Jagow-Klaff, 2001)
Thermal conductivity of water	λ_f	0.6	$Wm^{-1}K^{-1}$	(Jessberger & Jagow-Klaff, 2001)
Thermal conductivity of the saturated aquifer	λ_e	2	$Wm^{-1}K^{-1}$	calculated

4. RESULTS AND DISCUSSION

4.1. Statistical Model with SGemS

The model of the hydraulic conductivity distribution was realized with the *Stanford Geostatistical Modeling Software (SGeMS)*. The sequential Gaussian simulation algorithm permits the simulation of random fields. Based on a hard data file and a target histogram, 10 synthetic conductivity fields were created for each of the scenarios.

Table 8: Overview of the simulated scenarios

Scenario	σ^2_{logk}	mean logk	Nr. simulations
1	0.1	-3.86	10
2	0.5	-3.86	10
3	1	-3.86	10
4	3	-3.86	10

The input data of the field site was introduced in *SGeMS* in a point set file indicating the logarithmic hydraulic conductivity *(logk)* and the coordinates of measured points.

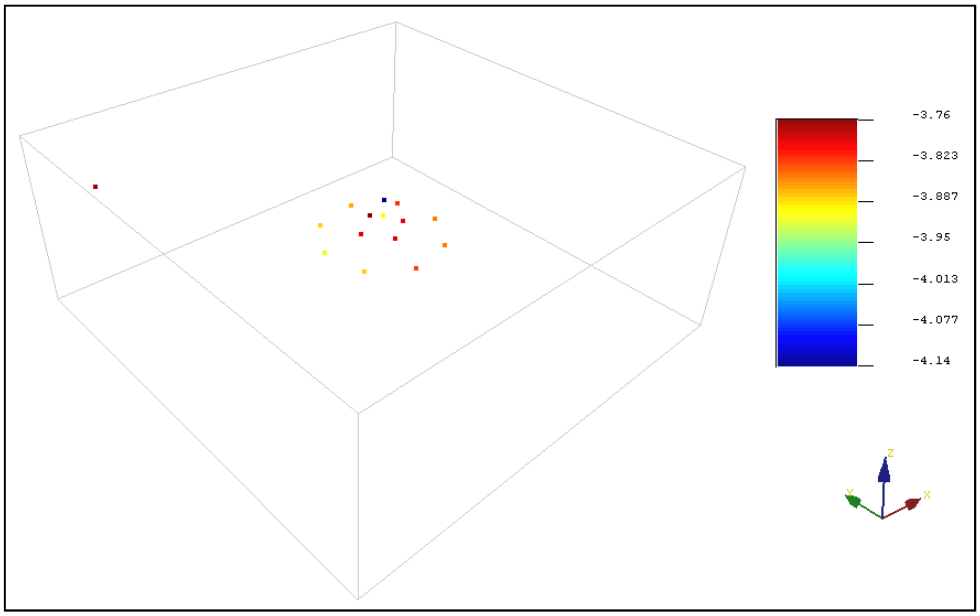

Image 8: Hard data (logk values measured in observation wells)

The target histogram was created with the *Data Analysis Tool* of *Excel.* With the function *Random number Generation* 1000 random numbers were generated to create the target histogram. A Normal distribution was chosen, the mean value was the logarithmic hydraulic conductivity obtained in the pumping test. 4 Target histograms were created introducing the standard deviations of the 4 simulated scenarios. Image 9 shows the histogram of the hard

data (measured hydraulic conductivity in the wells) and the generated target histogram for scenario 3 (σ^2_{logk}=1).

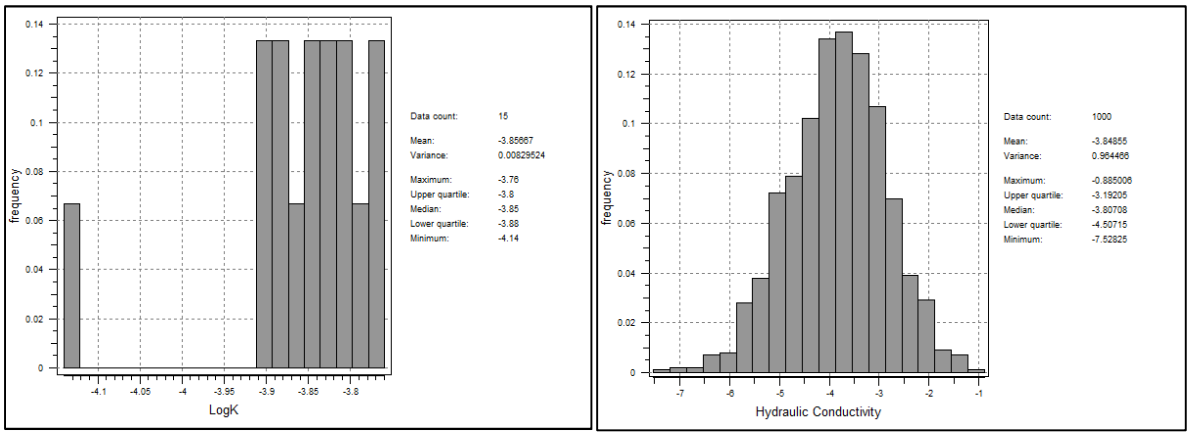

Image 9: Histogram of hard data and target histogram for σ^2_{logk}=1

To set up the statistical model, a carthesian grid of 100x100x40 was created in SGemS. The target histogram and the hard data file were loaded as objects for each of the scenarios. The function *Sequential Gaussian Simulation* in the algorithms panel was chosen to create the synthetic conductivity fields. All simulations were made using the same *Seed Number* and the same *Ranges* to compare the result of the scenarios.

In the algorithms panel all necessary data was introduced to run the simulations.

Table 9: Input Parameters for SGeMS for σ^2_{logk}=1

Input parameters for sgsim (σ^2_{logk}=1)			
General			
Nr. of simulations	10		
Seed Nr.	14071789		
Kriging Type	simple Kriging		
Data			
Max. cond. Data	15		
Ranges	30	30	30
Angles	50	0	0
Variogram			
Nugget effect	0		
Contribution	1		
Type	spherical		
Ranges	20	20	20
Angles	0	0	0

SGeMS saves all obtained simulations in the carthesian grid which was created before. Image 10 shows the histogram and conductivity field of scenario σ^2_{logk} =1 simulation 0.

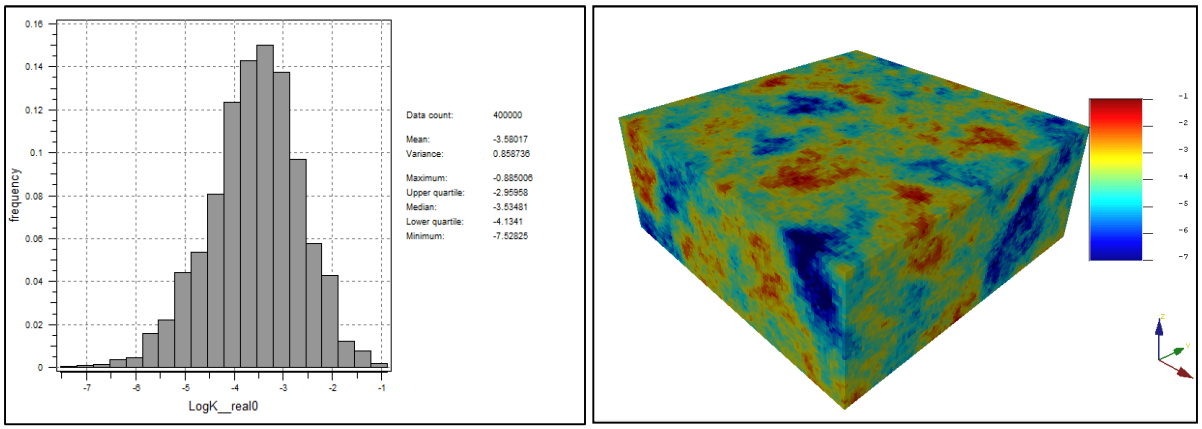

Image 10: Histogram and conductivity field of simulation 0 σ^2_{logk} =1

To export data from SGeMS, the objects can be saved as GS library files (gslib (“.”)) which can be edited in a normal text editor.

The same procedure was made to create 10 simulations for each scenario, hydraulic conductivity fields of simulations 0 are given in Image 11:

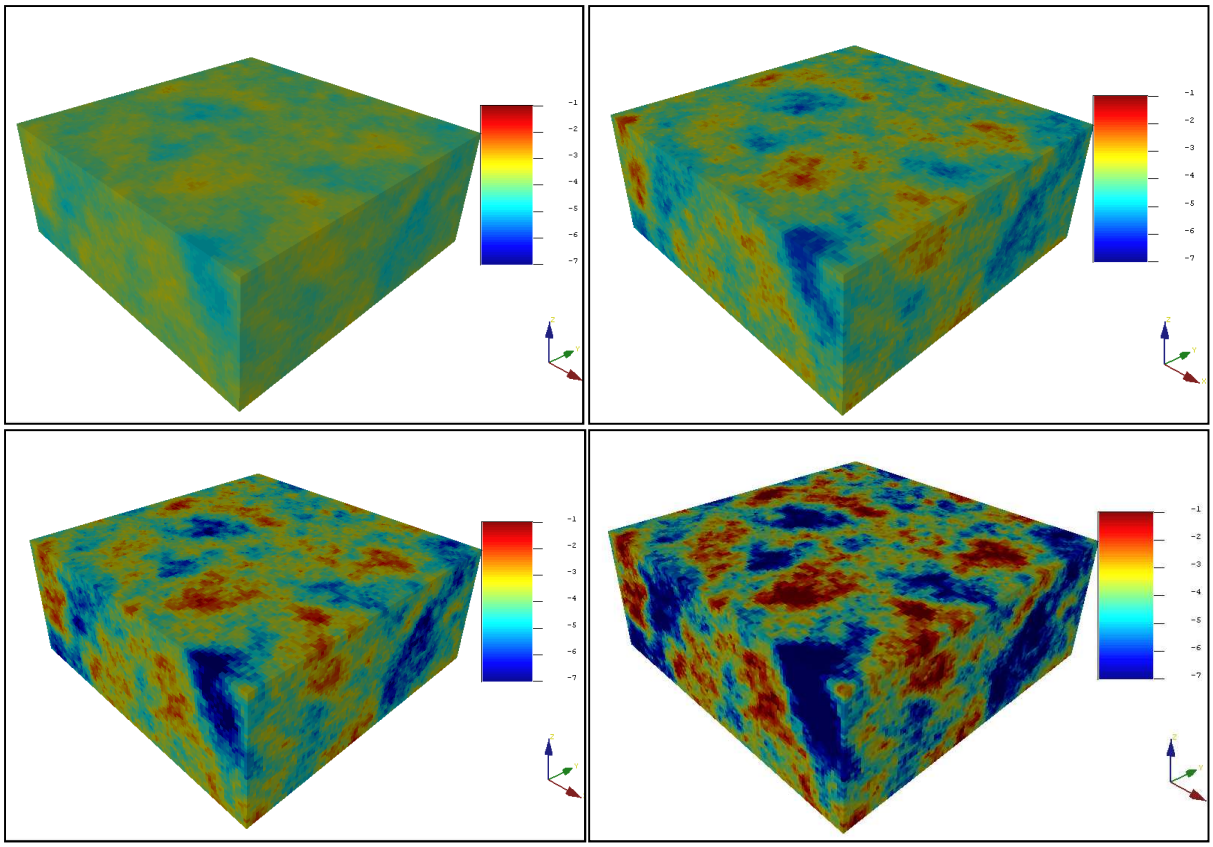

Image 11: Simulations 0 of σ^2_{logk} =0.1, σ^2_{logk} =0.5, σ^2_{logk} =1 and σ^2_{logk} =3

The data of each scenario was exported from SGeMS and edited in a text editor. The introduction of the SGeMS output files in PMWIN required a further formatting procedure with was made in MatLab 7.1 (Shuang Jin 2009).

4.2. Flow Model with ModFlow

The flow simulation was realized the finite difference flow model MODFLOW. 360 days steady state simulations were made with ModFlow to obtain the hydraulic head distributions of the 10 simulations of each scenario. To compare the obtained results a homogenous reference simulation was made.

Image 4 shows the hydraulic head distribution of layer 1 for the homogeneous case and fro simulation o of scenario 3 (σ^2_{logk} =1).

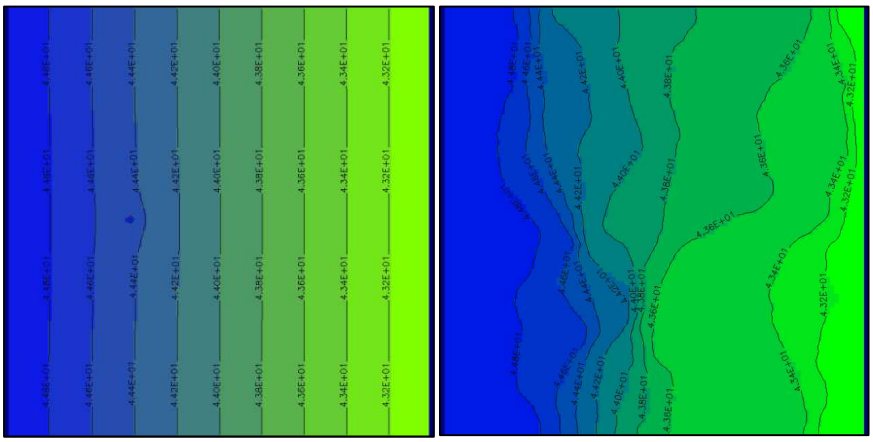

Image 12: Hydraulic head distributions in layer 1 for the homogeneous case and simulation 0 of σ^2_{logk} =1

ModFlow was not able to simulate the most heterogenic case of σ^2_{logk} =3 and cancels the simulation after the first time step. The other simulations show increasing heterogeneity of the hydraulic heads as the variance of the hydraulic conductivity increases.

The ModFlow file is used by MT3DMS to calculate the velocity field which is necessary for the heat transport simulation. ModFlow automatically creates the Flow file (.flo) for MT3D (Chiang & Kinzelbach, 1998).

4.3. Heat transport simulation with MT3DMS

The object of this section is to study the influence of heterogeneity of the parameters on heat transport simulation. An overall of 61 simulations were made to determinate the effect of the heterogeneity on the shape and development evolution of a temperature plume in a porous medium.

In a first step, heat transport simulations for the heterogenic hydraulic conductivity fields were made keeping the porosity and thermal conductivity constant. These simulations are compared with a homogenous reference simulation to show the changes in the heat plume dimensions caused by heterogeneity of the hydraulic conductivity k.

In the second step, heterogenic fields for all parameters (k, n, ρ_b, λ heterogeneous) were created and introduced to the model. The simulations of all scenarios are compared with each other to evaluate the influence of heterogeneity.

Table 1 gives an overview of the different simulations made in MT3DMS:

Table 10: Overview of all simulated scenarios

scenario 0 (σ^2_{logk} =0)	1 simulation	k homogenous
scenario 1 (σ^2_{logk} =0.1)	10 simulations	k heterogeneous / n, λ constant
	10 simulations	k, n, ρ_b, λ heterogeneous
scenario 2 (σ^2_{logk} =0.5)	10 simulations	k heterogeneous / n, λ constant
	10 simulations	k, n, ρ_b, λ heterogeneous
scenario 3 (σ^2_{logk} =1)	10 simulations	k heterogeneous / n, λ constant
	10 simulations	k, n, ρ_b, λ heterogeneous
scenario 4 (σ^2_{logk} =3)	-	-

Because of the lack of time for running more simulations, only 10 simulations were made for each scenario. For reliable conclusion at least 100 simulations should be made. This could be an outlook for future work.

4.3.1. Heterogenic hydraulic conductivity k distribution / constant porosity n and thermal conductivity λ distribution

To evaluate to influence of heterogeneity of hydraulic conductivity, simulations with heterogenic hydraulic conductivity distribution and constant porosity n and thermal conductivity λ distribution were made in MT3DMS. For each degree of variance 10 simulations were realized.

First a homogenous reference case was made using the hydraulic conductivity k mean value of Esseling site.

For the other scenarios the conductivity fields created in SGeMS were introduced to PMWIN layer by layer. The horizontal and vertical hydraulic conductivity were set equal to generate an isotropic aquifer. The implementation in PMWIN requires the ASCII format, so the GS library files had to be formatted. The formatting procedure was realized with MATLAB 7.1 (Shuang Jin 2009) and in a text editor.

Image 13 shows the simulation results for the evaluation of the heat plume after 360 days of injection for realizations 0 of scenario 0, 1, 2, and 3.

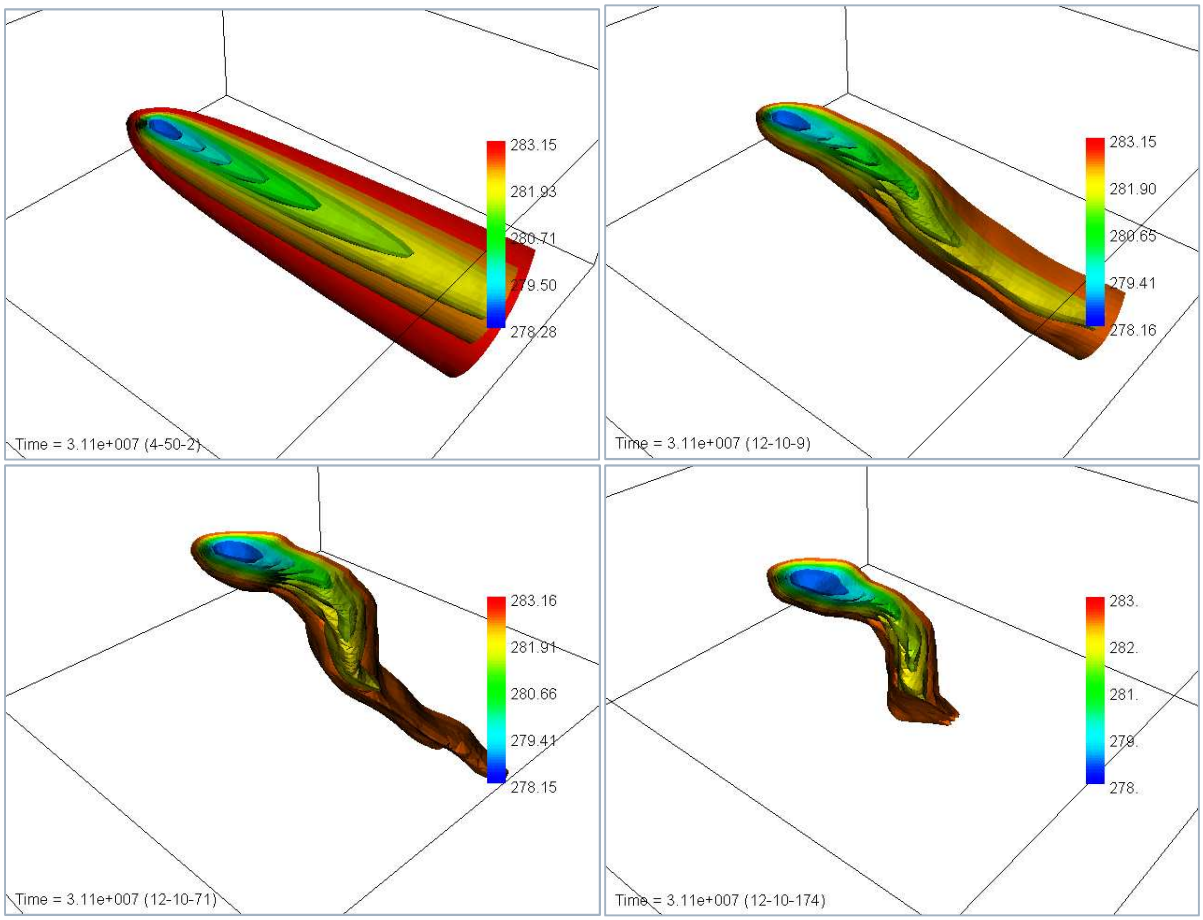

Image 13: Heat plume after 360 days of injection for simulations 0 of scenario 0, 1, 2, and 3

The results show that the increasing heterogeneity has an important effect on the shape of the temperature plume. Observing of the simulated cold plumes it can be concluded that increasing heterogeneity causes a decrease in the length and width.

To demonstrate the influence of heterogenic hydraulic conductivity on the cold plume development, simulated temperatures along the observation line (from the injection well downstream, 12m depth) were plotted in a diagram. Image 14 shows the temperatures along the observation line of simulation 0 for each scenario:

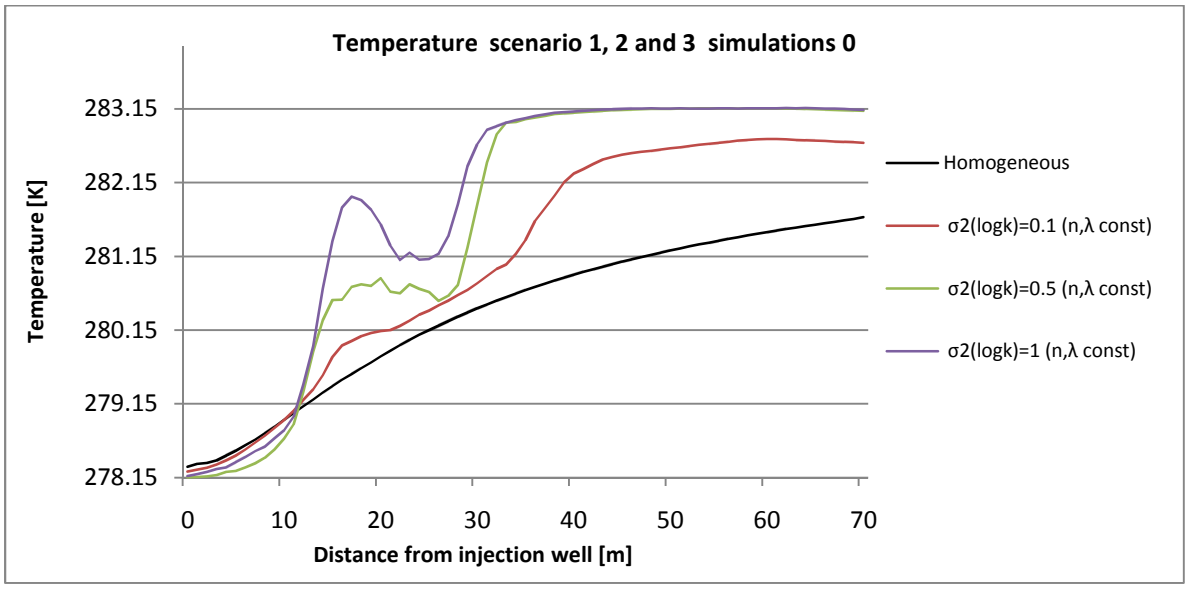

Image 14: Simulated temperatures along the observation line for scenario 0, 1, 2 and 3 simulations 0 (n, λ constant)

These first simulations already give an example how increasing heterogeneity affects on the temperature distribution. The simulated temperatures along the observation line diverge more and more from the homogenous case as the variance of k increases. This seems logical as water tends to flow to zones of higher permeability. The deviation of the cold plume in this model is mainly caused by predominating advective transport.

To compare the results, the mean of the 10 realizations made for each scenario was calculated and plotted in a diagram. Image 15 and Image 16 show the 10 simulations and the mean (red line) of scenario 1 (σ^2_{logk} =0.1) and scenario 3 (σ^2_{logk} =1) (n, λ constant).

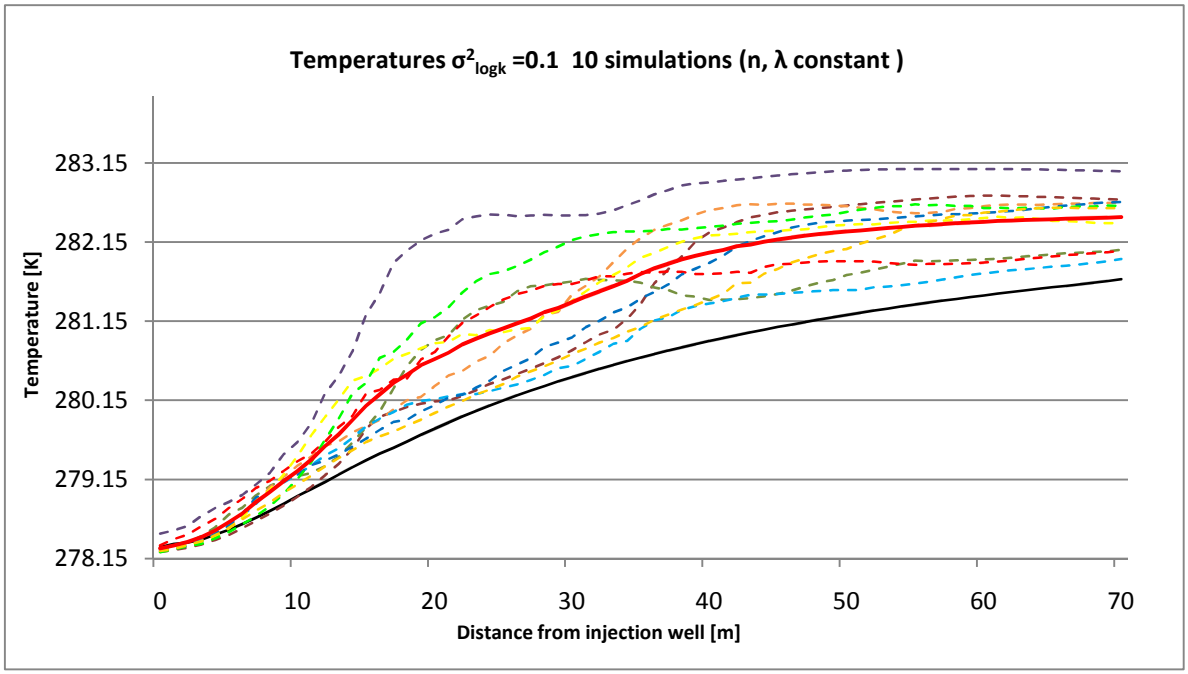

Image 15: Simulated temperatures for the 10 simulations of σ^2_{logk}=0.1 (n, λ constant) and the calculated mean (red line)

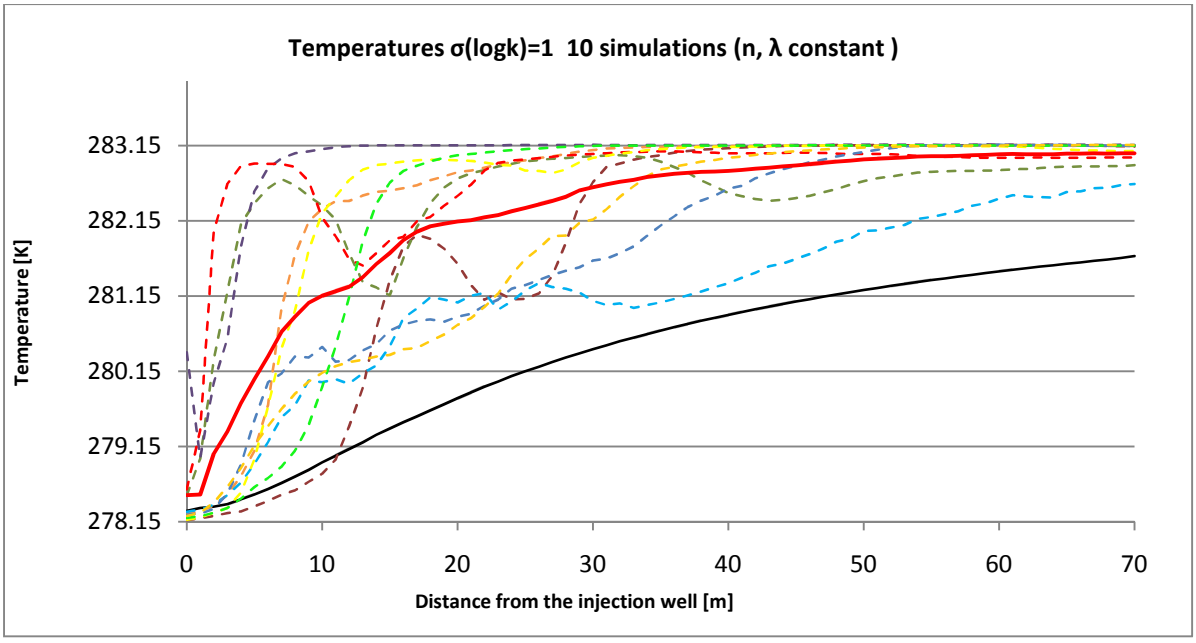

Image 16: Simulated temperatures for the 10 simulations of σ^2_{logk}=1 (n, λ constant) and the calculated mean (red line)

As we can see in the diagrams, the mean values of 10 simulations diverge more from the homogenous case as variance of k increases. Also the single simulations for each scenario show a rising variability as variance of k increases. This causes rising uncertainty in the prediction of the cold plume development and extension. Image 17 compares the calculated mean values of the 10 simulations made for each scenario.

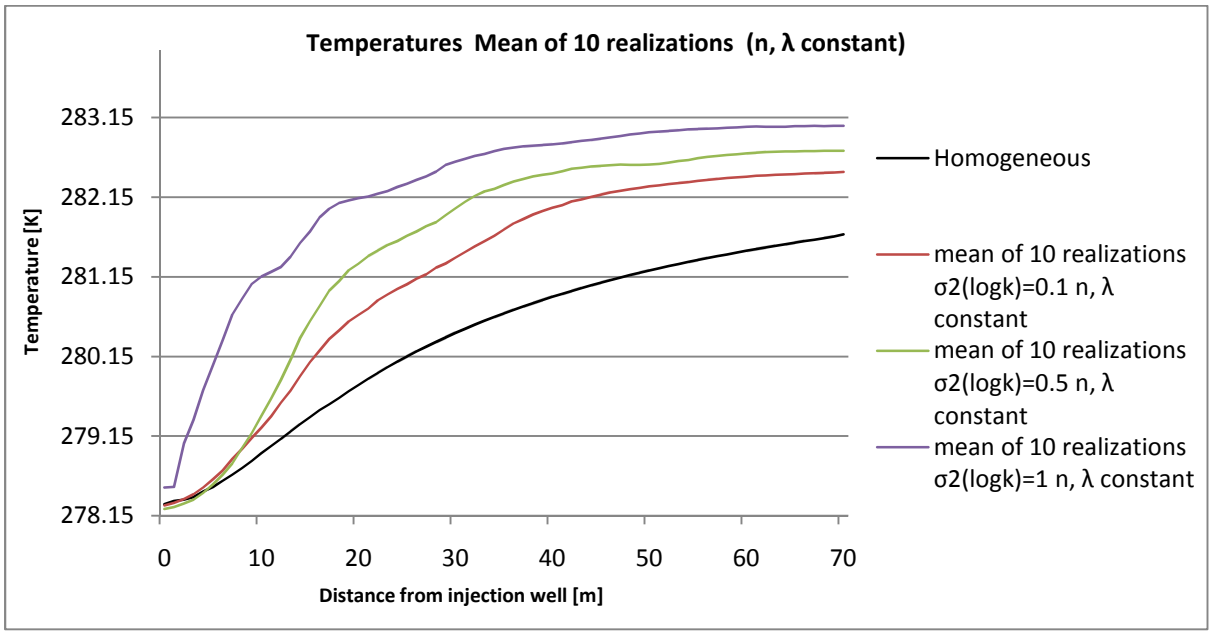

Image 17: Mean of 10 simulations for scenario 0, 1, 2, 3

Results show how the heterogeneity of permeability affects on the evaluation of the heat plume. A higher variance in hydraulic conductivity distribution causes an important variability in the simulated temperature field. A relatively small change in heterogeneity of k causes a considerable uncertainty in the prediction of the heat distribution in the aquifer system.

Similar conclusions were made in former works on this topic. Bridger and Allen discovered that heat moves preferentially through layers of higher conductivity in the aquifer (Bridger & Allen, 2010). Another conclusion was made by Hidalgo who found out that heterogeneity in permeability has a dispersive effect on the temperature plume (Hidalgo, 2009). The same conclusion was made by Shuang Jin (Shuang, 2009). Fergusen found out that even small amounts of heterogeneity in the hydraulic conductivity field can result in considerable uncertainty in the distribution of heat in the subsurface in thermal developments of ground water resources. Furthermore he concluded that less heat can be recovered from heterogeneous aquifers than from homogeneous ones (Ferguson, 2007).

It can be concluded that heterogeneity in permeability results in significant changes in the configuration of the temperature plume. Furthermore it causes uncertainty in the prediction of heat distribution in the subsurface. If the exact configuration of the temperature plume is of interest, the heterogeneity in permeability has to be implemented in the transport simulation.

4.3.2. Heterogenic hydraulic conductivity k, porosity n and thermal conductivity λ distribution

The object of this chapter is the evaluation of the influence of heterogeneity of all parameters on heat transport simulation. Therefore 10 simulations for each scenario were realized implementing heterogenic permeability, porosity and thermal conductivity fields. The idea was to calculate the porosity n from the logarithmic hydraulic conductivity files created with SGeMS for each cell. The new porosity files were then used to calculate the other parameters like bulk density and thermal conductivity and in a further step the molecular dispersion coefficient.

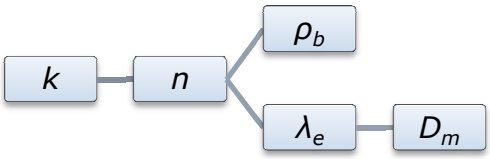

In the first step porosity n was calculated from the logarithmic hydraulic conductivity for each cell. In chapter 2.1.3 various empirical relationships between hydraulic conductivity k and porosity are presented. Calculations applying different formulas were made and the obtained results were compared with each other. Finally the formula of Busch and Luckner (1993) was used to calculate the porosity from the hydraulic conductivity files of:

$$n = 0.05 \cdot logk + 0.4$$

One reason to apply this formula was the simple linear relationship with few parameters which avoids further errors due to introduction of empirical parameters. The other reason was that the obtained results where the closest to the mean value of the field site. Image 18 shows the calculated porosities n. The visualization of the calculated files was realized with the graphical interface of SGeMS.

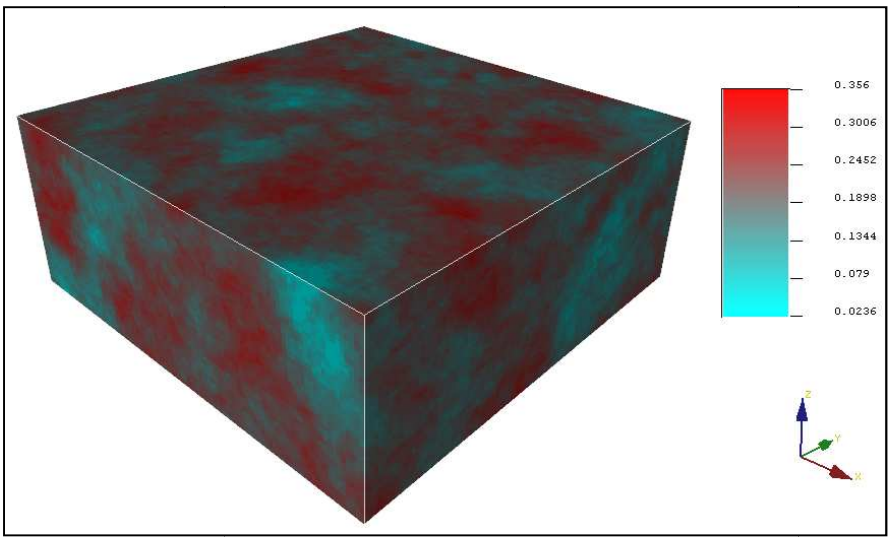

Image 18: Heterogeneous porosity distribution (σ^2_{logk}=1 simulation 0)

The obtained porosity matrix were saved in ASCII files and introduced to PMWIN layer by layer.

Another parameter which is affected by the change of the porosity is the bulk density ρ_b. It is used by MT3DMS to calculate the retardation factor R.

$$R = \left(1 + \frac{\rho_b K_d}{n}\right)$$

The bulk density ρ_b was calculated from the porosity files using the formula

$$\rho_b = (1 - n) \cdot \rho_s$$

In which the ρ_s is the density of the solid. The obtained files were introduced to MT3DMS for each layer. Image 19 shows the bulk density distribution, the visualization was realized with the graphical interface of SGeMS.

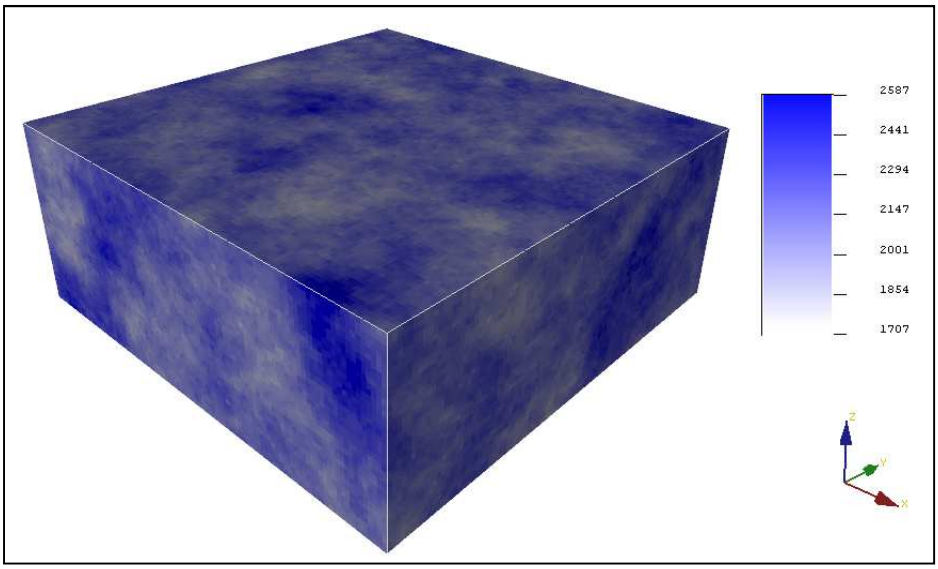

Image 19: Heterogenous bulk density ρ_b distribution (σ^2_{logk} =1 realization 0)

Finally, the thermal conductivity λ was calculated from the porosity file. The calculation was realized applying the geometric mean formula for a saturated aquifer presented in Chapter 2.2.1.

$$\lambda_{sat} = {\lambda_s}^{1-n} \cdot {\lambda_w}^{n}$$

To implement the thermal conductivity to MT3DMS the new effective molecular diffusion coefficient had to be calculated using the relationship between thermal conductivity and molecular diffusion coefficient developed in Chapter 2.3.3:

$$D_m = \frac{\lambda_e}{n \cdot \rho_f c_f}$$

Image 20 shows the thermal conductivity λ distribution and the effective molecular diffusion coefficients, visualized in the graphical interface of SGEMS.

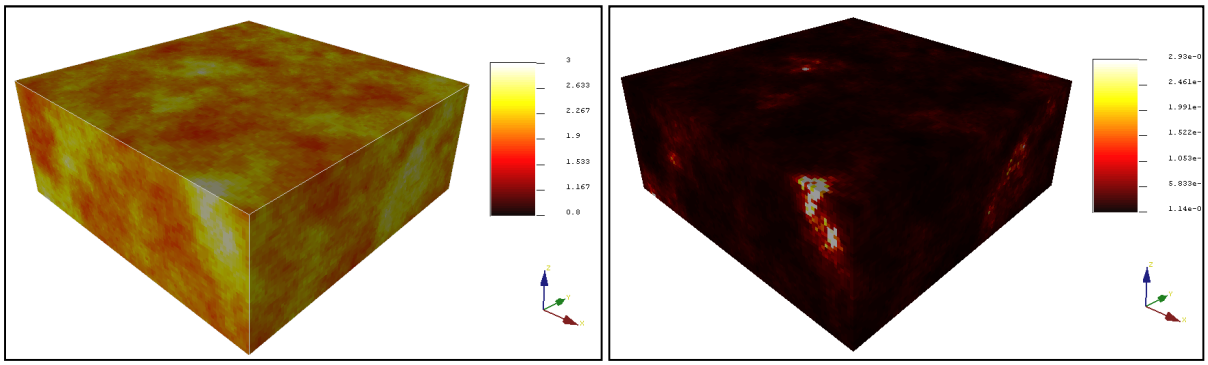

Image 20: Heterogeneous thermal conductivity λ distribution and the effective molecular diffusion coefficient distributions (σ^2_{logk}=1 simulation 0)

The PMWIN package only permits the introduction of the effective molecular diffusion coefficient layer by layer. For this reason the mean of each layer was calculated and implemented in the Dispersion package of MT3DMS.

Simulations for all scenarios and realizations were made, implementing the heterogeneous fields of hydraulic conductivity k, porosity n, bulk density ρ_b and thermal conductivity λ. The obtained results were compared to the simulations of chapter 4.3.1 to evaluate the importance of the changes made in porosity n, bulk density ρ_b and thermal conductivity λ. Like before in the homogenous case the hydraulic conductivity was set to the mean value of Esslingen site. Image 21 and Image 22 show the simulation results for the evaluation of the heat plume after 360 days of injection for the two cases of σ^2_{logk}=1 simulation 0.

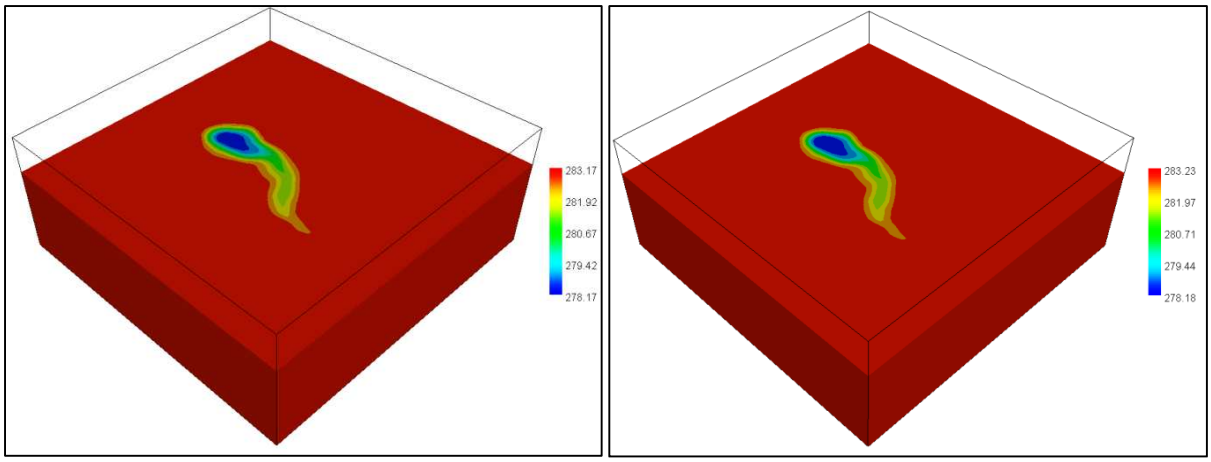

Image 21: Simulated temperature plume for σ^2_{logk}=1 simulation 0 (n, λ constant on the left / n, λ heterogeneous on the right) cropped at Z=0.7

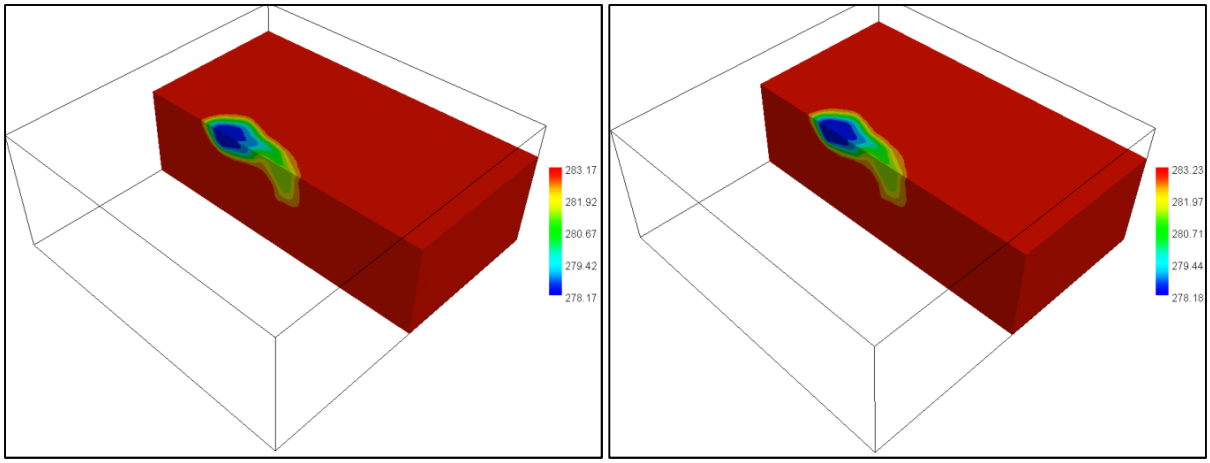

Image 22: Simulated temperature plume for σ^2_{logk} =1 simulation 0 (n, λ constant on the left / n, λ heterogeneous on the right) cropped at Y=0.5 and Z=0.7

A first observation of the 2 simulations doesn´t show any differences in form and development of the temperature plume in the 2 simulations. This may be due to the predominating advective transport. The dispersive transport seems to be less important. Small variations in the simulations can be observed in the zones of cold water close to the injection well which seem to be larger in the all heterogeneous case on the right hand side.

To compare the results, the mean of the 10 simulations made for each scenario was calculated and plotted in a diagram. Image 23 and Image 24 show the 10 simulations and the mean (red line) of scenario 1 (σ^2_{logk}=0.1) and scenario 3 (σ^2_{logk}=1) (n, λ heterogeneous).

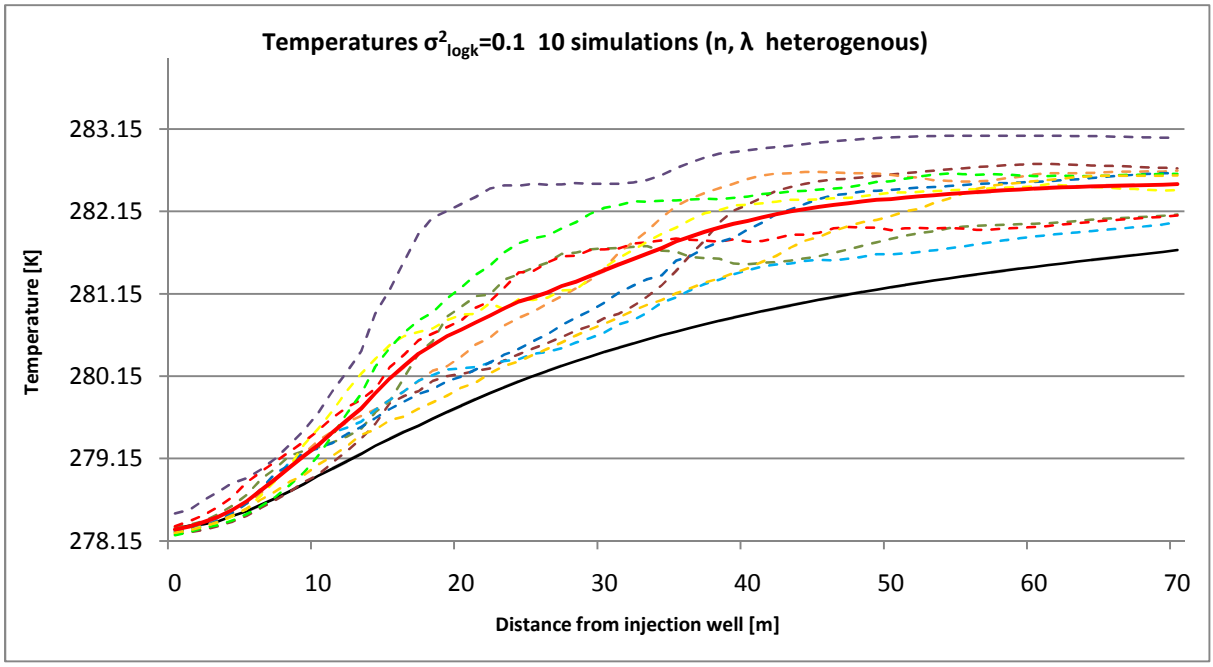

Image 23: Simulated temperatures for the 10 simulations of σ^2_{logk}=0.1 (n, λ heterogeneous) and the calculated mean (red line)

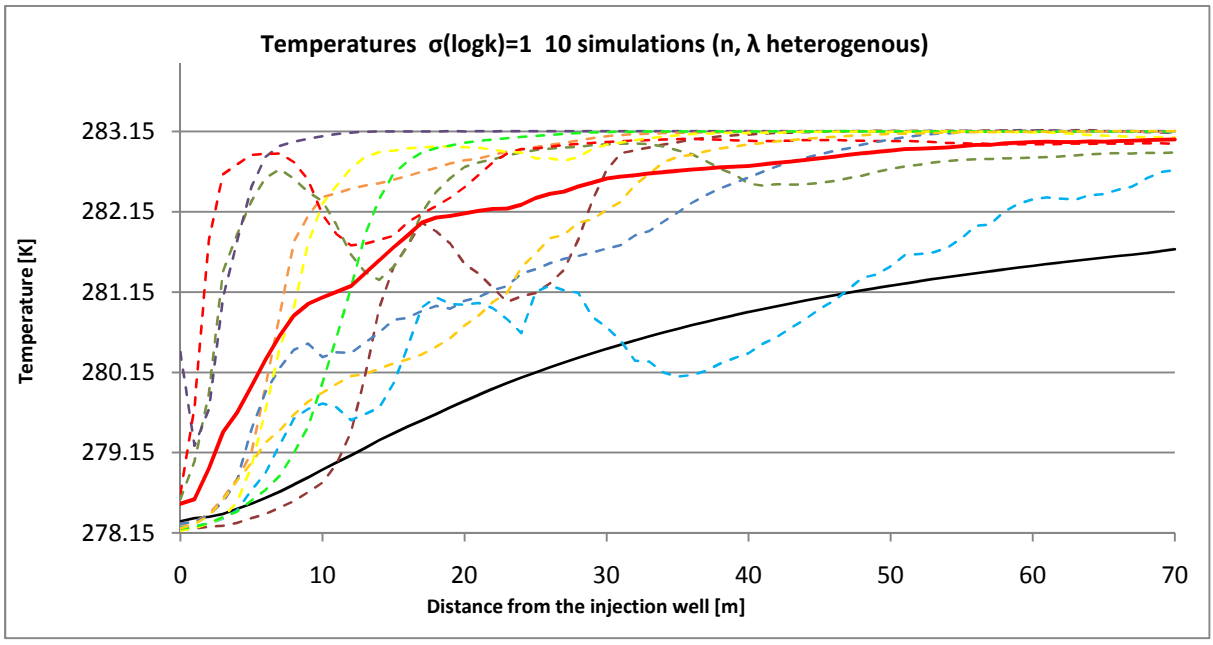

Image 24: Simulated temperatures for the 10 simulations of σ^2_{logk}=1 (n, λ heterogeneous) and the calculated mean (red line)

The simulated temperature profiles along the observation line seem to be very close to the ones shown in the previous chapter. The variability of the single simulations is mainly caused by the heterogeneity of the permeability and the other parameters have a minor influence.

Image 25 compares the calculated mean values of the 10 simulations made for each scenario for n, λ constant and n, λ heterogeneous.

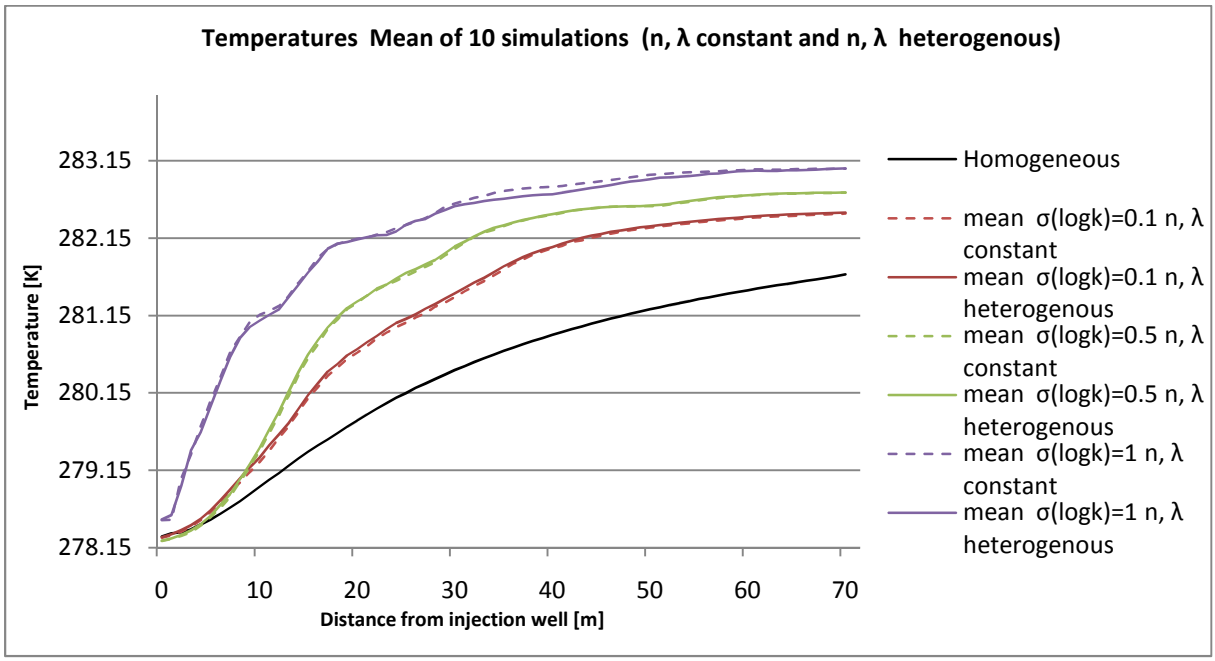

Image 25: Mean of 10 simulations for scenario 0, 1, 2, 3 (n, λ constant t / n, λ heterogeneous)

As expected the two mean curves of 10 simulations for the two cases are almost identical. The mean curves of scenario 3 (σ^2_{logk}=1) show slight differences, the other scenarios do not show any variability caused by the heterogeneity of the porosity and thermal conductivity. An explanation for this phenomenon could be the relatively high hydraulic gradient. Due to the high flow velocities advection is the predominating form of transport in the simulations of this work. Dispersive transport has a minor importance and the effects of the changes made in porosity and thermal conductivity are insignificant.

The results of all simulations of scenario 1 and scenario 3 are presented in Image 26 and Image 27.

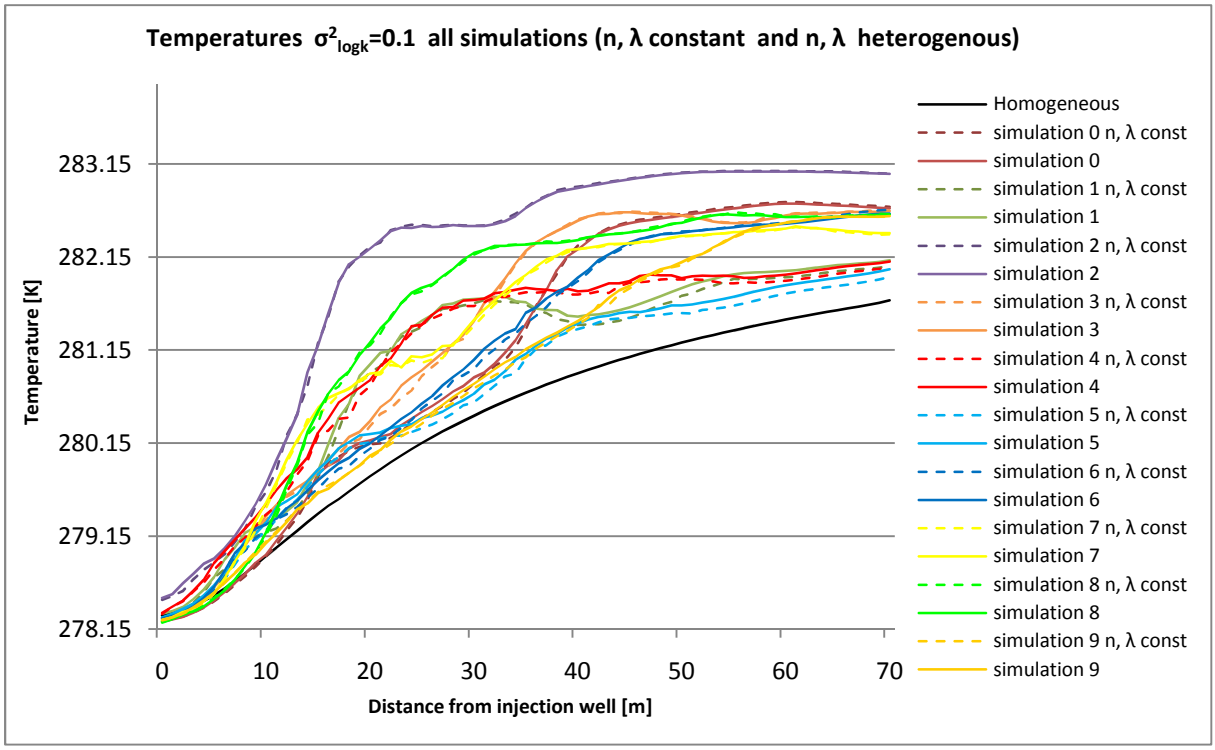

Image 26: Simulated temperatures for the 10 simulations of σ^2_{logk} =01 (n, λ constant / n, λ heterogeneous)

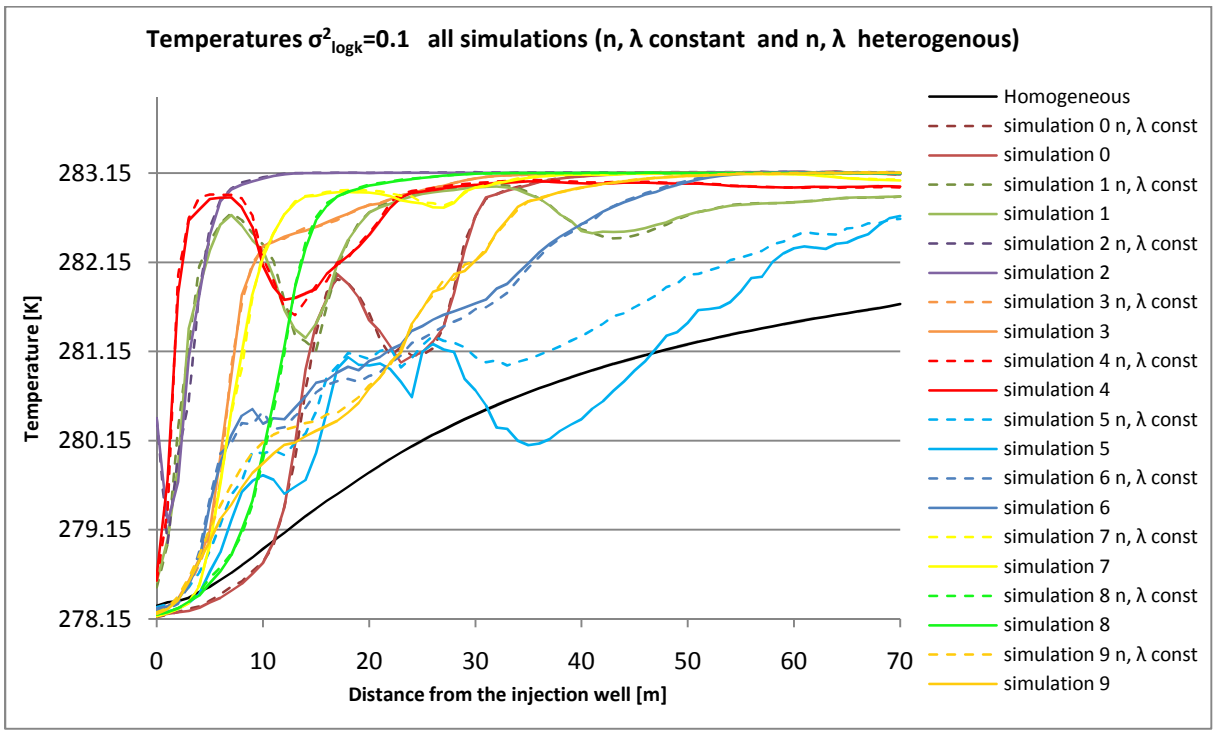

Image 27: Simulated temperatures for the 10 simulations of σ^2_{logk} =1 (n, λ constant / n, λ heterogeneous)

Comparing the two cases (n, λ constant and n, λ heterogeneous) of each single simulation it can be observed that the difference between the two cases increases slightly with increasing heterogeneity. Some simulations made for scenario 3 (σ^2_{logk}=1) show temperature

differences up to 1 ℃. The highest differences sho w the simulations which are close to the homogeneous case. It seems that, like mentioned before, the distribution of the temperature slightly changes in the all heterogeneous case and zones of low temperature are longer in flow direction.

This effect could be much stronger in cases of low hydraulic gradient. As flow velocities get lower with decreasing gradient, the influence of dispersion get higher and changes in thermal conductivity and porosity could have a major effect on plume evaluation. Other simulations should be made using different hydraulic gradients to investigate the influence of heterogeneity in combination with the hydraulic gradient.

4.3.3. Variances of the temperatures

To quantify the uncertainty in the prediction of temperature distribution caused by heterogeneity of the parameters, the variance of the simulated temperature plumes for the 10 simulations was computed for all scenarios. Because of problems exporting the ASCII-Matrix files from PMWIN, the temperatures in layer 13 and row 50 were saved manually with the Results Extractor. With these files the variances of the simulated temperature were calculated and visualized with the graphical interface of SGeMS. The implementation of the MT3DMS results to SGeMS required a formatting and reshaping procedure which was made in MATLAB 7.1.

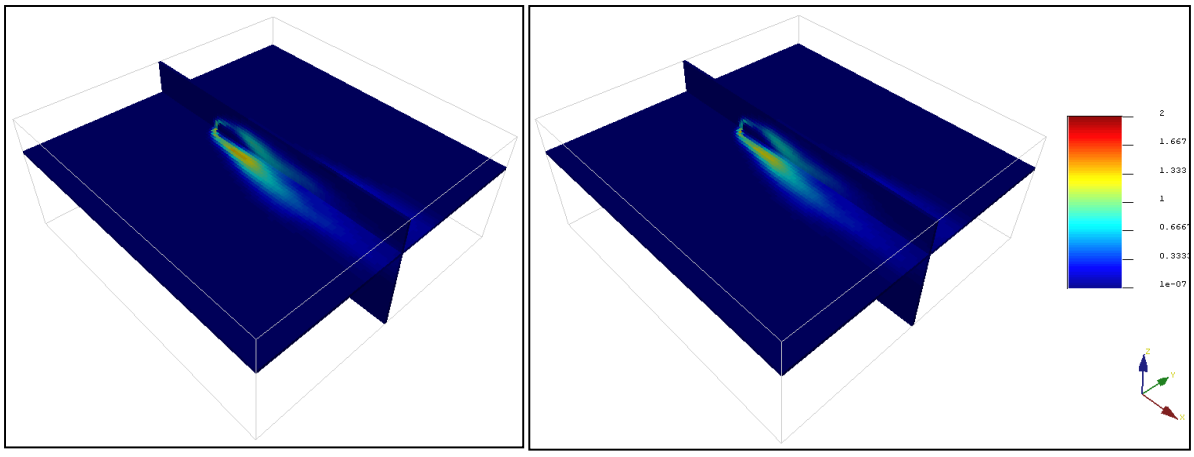

Image 28: Variance of the temperatures in layer 13 / row 50 of the 10 simulations of σ^2_{logk} =0.1 (n, λ constant on the left / n, λ heterogeneous on the right)

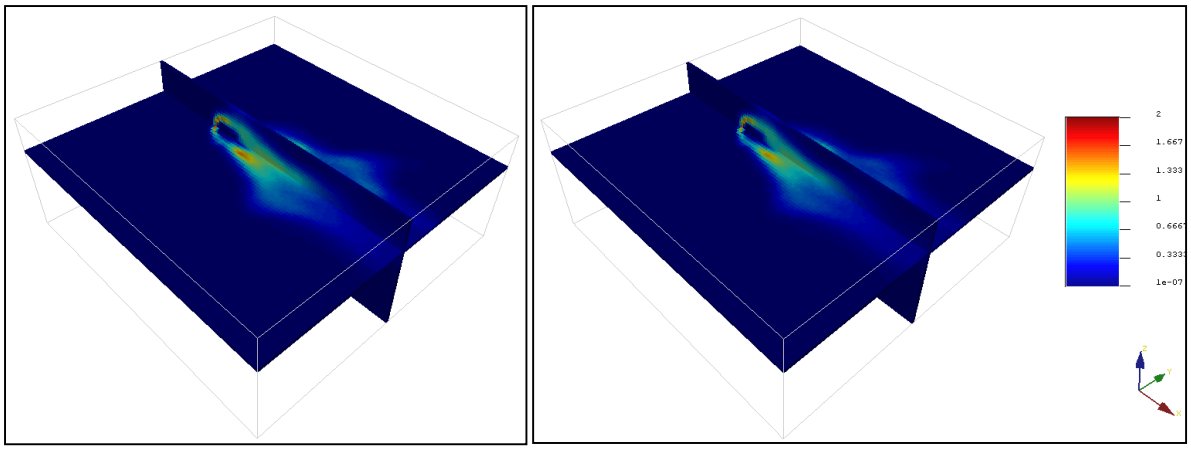

Image 29: Variance of the temperatures in layer 13 / row 50 of the 10 simulations of σ^2_{logk} =0.5 (n, λ constant on the left / n, λ heterogeneous on the right)

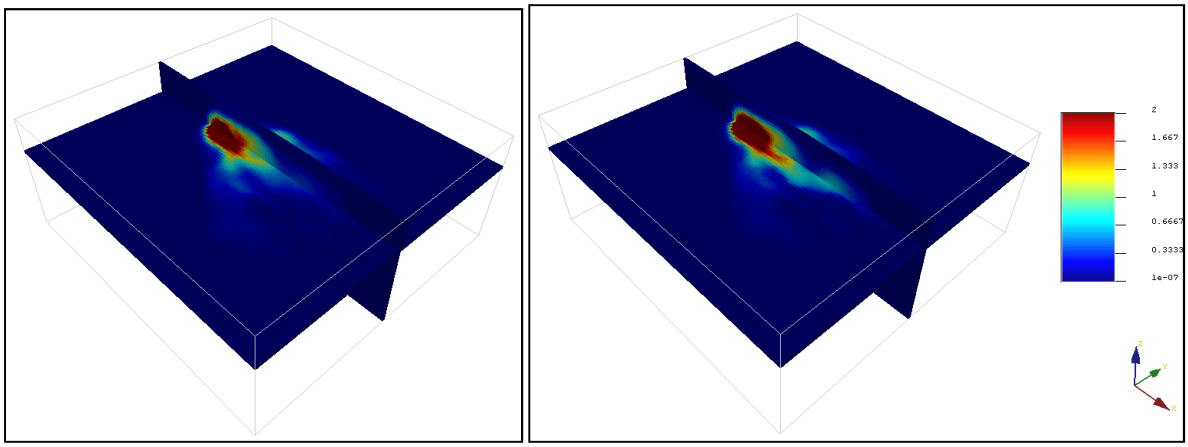

Image 30: Variance of the temperatures in layer 13 / row 50 of the 10 simulations of σ^2_{logk} =1 (n, λ constant on the left / n, λ heterogeneous on the right)

Results show that an increasing variance of permeability causes increasing variance in the expected temperature distribution. Scenario 3 (σ^2_{logk} =1) shows considerably higher variances than scenario 1 (σ^2_{logk} =0.1). Generally the highest variances can be observed in the first 20 meters from the injection well. The changes in flow direction generate an uncertainty in the prediction of the temperature plume.

Image 28 and Image 29 present the calculated variance of simulated temperatures for scenario 1 (σ^2_{logk} =0.1) and scenario 2 (σ^2_{logk} =0.5). The variance of temperatures close to the injection point is very low due to the constant injection rate and temperature. The highest variances can be observed at about 15 to 20 meters from the injection well. Comparing the calculated variances for the 2 cases (n, λ constant on the left / n, λ heterogeneous on the right) no major difference can be observed.

The calculated variance for the most heterogenic case (σ^2_{logk} =1) is presented in Image 30. The highest variances can be found close to the injection point up to about 10 to15 meters in

flow direction. Abrupt changes in permeability result in concentrated narrow heat plumes which generates increasing variance in temperature distribution.

Comparing the calculated variances for the simulated temperatures of scenario 3 (σ^2_{logk} =1) for the 2 cases (n, λ constant on the left / n, λ heterogeneous on the right) an increase in variance in the all heterogeneous case can be found. The introduction of the heterogeneous porosity and thermal conductivity fields provokes a rising uncertainty especially in flow direction.

This shows that the consideration of the heterogeneity of the porosity n and thermal conductivity λ could be important for heat transport simulation in highly heterogeneous systems. It is possible that, in combination with a low hydraulic gradient, high heterogeneity of the porosity n and thermal conductivity λ could cause a considerable increase in the uncertainty in the prediction of the temperature plume.

Like mentioned before only 10 simulations were made to calculate the variance in the temperature distribution. This is not enough to make reliable conclusions. At least 50 to 100 simulations should be made. Because of the time limitation it was not possible to do that.

5. CONCLUSIONS AND FUTURE WORK

This work was made on order to get further information about heat transport simulation in shallow geothermal systems. The main objectives were:

- Analysis of the influence of heterogenic permeability distribution on heat transport simulations in shallow geothermal systems.
- Analysis of the influence of heterogenic permeability, porosity, bulk density and thermal conductivity distributions on heat transport simulations in shallow geothermal systems.

To link the investigation to a practical application, model dimension and aquifer parameters were chosen considering a report on a field study realized in Germany. A total amount of 61 simulations were made, implementing homogenous and heterogeneous permeability, porosity and thermal conductivity fields to evaluate the influence of heterogeneity of the parameters on heat transport. Following conclusions can be taken:

- Heterogeneity in the hydraulic conductivity field causes significant changes in the hydraulic head distribution. This affects the flow velocity field which is used for heat transport simulation.
- Heterogeneity of hydraulic conductivity has a major influence on the shape and development of a temperature plume in a porous media. A high degree of variance in the logarithmic hydraulic conductivity distribution results in a rising variability of the simulated temperature fields and a considerable uncertainty in the prediction of the temperature distribution in an aquifer system. The calculated variances of the simulated temperature fields between are rising significantly with increasing degree of variance in the permeability field.
- Heterogeneity in permeability distribution causes changes in the shape and configuration of the temperature plume. The length and width of the plume decreased as the variance of the permeability increases.
- The zones of cold water seem to be more concentrated, dispersion gets less important due to the higher flow velocities in the pore channels. This phenomenon is widely known as “channeling effect”.
- The heterogeneity of porosity and thermal conductivity seems to have less impact on modeling results than the one of permeability. Low heterogeneity degrees in the porosity and thermal conductivity distribution do not cause important changes in shape and development of the simulated temperature plume. The calculated temperature mean values along an observation line seem to be identical.

- Higher degrees of heterogeneity in porosity and thermal conductivity distributions show slight differences between the simulations made with homogenous and heterogeneous porosity and thermal conductivity. In the most heterogeneous case (σ^2_{logk}=1) the calculated variance of the simulated temperatures increases significantly when considering the calculated porosity and thermal conductivity fields.

Former works on this topic showed similar results. Fergusen concluded that even small heterogeneities in the hydraulic conductivity fields can result in considerable uncertainty in the distribution of heat in the subsurface in thermal developments of ground water resources. Furthermore he concluded that less heat can be recovered from heterogeneous aquifers than from homogeneous ones (Ferguson, 2007).

Bridger and Allen discovered that heat moves preferentially through layers of higher conductivity in the aquifer (Bridger & Allen, 2010). Another conclusion was made by Hidalgo who found out that heterogeneity in permeability has a dispersive effect on the temperature plume (Hidalgo, 2009). The same conclusion was made by Shuang Jin. Furthermore she investigated the influence of porosity and thermal conductivity heterogeneity. In her report she concluded that porosity and thermal conductivity showed minor importance (Shuang, 2009).

It can be concluded that heterogeneity in permeability results significant changes in the configuration of the temperature plume. Furthermore it causes uncertainty in the prediction of heat distribution in the subsurface. If the exact configuration of the temperature plume is of interest, the heterogeneity in permeability has to be implemented in the transport simulation.

On the other hand heterogeneity of porosity and thermal conductivity showed to be less important in this model. Higher degrees of heterogeneity showed slight differences in cold plume shape and in the calculated temperature variance. Main reason for this could be the predominating advective transport. The assumed hydraulic gradient turned out to be very high and heat transport is driven mainly by the motion of the groundwater. For further conclusions simulations with different hydraulic gradients should be made.

For the results presented in this work, 10 simulations for each degree of heterogeneity have been made so far. To take reliable conclusions at least 50-100 simulations for each scenario should be made. Furthermore simulations with different hydraulic gradients should be made. A lower hydraulic gradient causes lower flow velocities and advective transport becomes less important. This leads to an increasing importance of dispersive transport. As porosity and thermal conductivity are used to calculate the dispersion term, the heterogeneity of these parameters could have a significant influence.

6. REFERENCES

Anderson, M. O., & Woessner, W. W. (1992). *Applied Groundwater Modeling.* San Diego: Academic Press.

Anderson, M. P. (2005, Vol 43 No.6). Heat as a Ground Water Tracer. *Ground Water* , pp. 951-968.

AQTESOLVE. (2011). *summary_of_solutions*. Retrieved 5 16, 2011, from aqtesolv.com: www.aqtesolv.com/summary_of_solutions.htm

Armstrong, F., & Blundell, K. (2007). *Energy ...beyond oil.* Oxford: Oxford University Press.

Balke, K., & Brenner, K. (1980). *Hydrothermische Versuchsfelder 1+2.* Dortmund: VEW AG.

Banks, D. (2008). *An introduction to Thermogeology / Ground source heating and cooling.* unknown: Blackwell Publishing.

Bear, J. (1972). *Dynamics of fluids in porous media.* New York: American Elsevier Publishing Company.

Bear, J., & Cheng, A. (2010). *Modeling Groundwater Flow and Contaminant Transport.* New York: Sprenger.

Bridger, D., & Allen, D. (2010, 47). Heat transport simulations in a heterogeneous aquifer used for aquifer thermal energy storage (ATES). *Canadian Geotechnik Jounal* , pp. 96-115.

Busch, K.-F., & Luckner, L. (1993). *Geohydraulik Band 3 von Lehrbuch der Hydrogeologie.* Gebr. Borntraeger.

Canada, N. R. (2009, 04 20). *Heating_and_Cooling_with_a_Heat_Pump.* Retrieved 06 15, 2011, from http://oee.nrcan.gc.ca: http://oee.nrcan.gc.ca/publications/infosource/pub/home/Heating_and_Cooling_with_a_Heat_Pump_Section4.cfm

Carman, P. (1937). Fluid flow through a granular bed. *Trans. Inst. Chem. Eng.* , 150-167.

Carrier, D. W. (2003). Good by Hazen; Hello Kozeny-Carman. *Journal of Geotechnical and Geoenvironmental Engineering Vol. 129* , 1054-1056.

Chiang, W.-H., & Kinzelbach, W. (1998). *Processing Modflow.*

Christensen, J. (2006). *Renewable Energy to Climate Change Solutions.* Paris: Renewable Energy Policy Network for the 21st Century (REN21).

Conde Lázaro, E., & Ramos Millán, A. (2009). *Guía Técnica de Bombas de Calor Geotérmicas.* Madrid: Gráficas Arias Montano, S.A.

Corapcioglu, M. Y. (1996). *Advances in porous medium.* Amsterdam: Elsevier sience B.V.

Costa, A. (2005). Permeability-Porosity relationship: A reexamination of the Kozeny Carman equation based on fractal pore space geometry assumption. *Geophysical research letters Vol. 33* , 1-5.

Dunn, D. (unknown). *thermodynamics.* Retrieved 06 15, 2011, from www.freestudy.co.uk: http://www.freestudy.co.uk/thermodynamics/t5201.pdf

Dvorkin, J. (2009). *KOZENY-CARMAN EQUATION REVISITED.* unknown: unknown.

Energy, U. d. (2011, 02 09). *Space Heating and Cooling*. Retrieved 05 27, 2011, from www.energysavers.gov: www.energysavers.gov/your_home/space_heating_cooling/index.cfm/mytopic=12650

engineeringtoolbox. (n.d.). *Specific-heat-capacity.* Retrieved 2 2011, from engineeringtoolbox.com: http://www.engineeringtoolbox.com/specific-heat-capacity-d_391.html

engineeringtoolbox. (n.d.). *www.engineeringtoolbox.com.* Retrieved 3 4, 2011, from Solids-Specific heats: www.engineeringtoolbox.com/specific-heat-solids-d_154.html

ETI-Brandenburg. (2010). *Oberflächennahe Geothermie.* Retrieved 06 03, 2011, from www.eti-brandenburg.de: http://www.eti-brandenburg.de/energiethemen/geothermie/oberflaechennahe-geothermie.html

Ferguson, G. (2007, July/August). Heterogeneity and Thermal Modeling of Ground Water. *Ground Water* , pp. 485-490.

GeoproDesign. (2009). *residential-geothermal-basics.* Retrieved June 06, 2011, from www.geoprodesign.com: http://www.geoprodesign.com/en/Page/residential-geothermal-basics

Gleason, C. (2008). *Geothermal Energy: using earth furnance.* New York: Craptree Publishing Company.

Hazen, A. (1893). Some Physical Properties of Sands and Gravels with Special Reference to their Use in Filtration. *24th Annual Report, Massachusetts State Bureau of Health, Publ. Doc. 34* , pp. 539–556.

Hidalgo, J. J. (2009, August). Steady state heat transport in 3D heterogeneous porous media. *Advances in Water Resources* , pp. 1206-1212.

Hu, B. X. (2009). Examining the influence of heterogeneous porosity fields on conservative solute transport. *Journal of Contaminant Hydrology 108* , 77-88.

Jessberger, H. L., & Jagow-Klaff, R. (2001). *Grundbau Taschenbuch/ Teil2: Technische Verfahren.* Berlin: Ernst&Sohn Verlag.

Jiji, L. M. (2009). *Heat conduction.* Heidelberg: Springer Verlag.

Kasenow, M. (2001). *Applied Groundwater Hydrology and Well Hydraulics.* Denver: Water Resources Publication LLC.

Kaviany, M. (2001). *Principles of heat transfer in porous Media.* Springer.

Kozeny, J. (1927). *Über kappilare Leitung des Wassers im Boden.* Wien: Hölder-Pichler-Tempsky, A.-G. [Abt.:] Akad. d. Wiss.,.

Krumbein, W., & Monk, G. (1942). Permeability as a function of size parmeters of unconsolidated sand. *American institude of mining Littleton CO* , 153-163.

Kulasiri, D., & Verwoerd, W. (1992). *Stochatic Dynamics modeling solute transport in porous media.* Amsterdam: Elsevier Science B.V.

Kupfersberger, H. (2009, 59). Heat transfer modelling of the Leibnitzer Feld aquifer, Austria. *Environ Earth Sci* , pp. 561-571.

LLOPIS TRILLO, G., & LÓPEZ JIMENO, C. (2009). *Guía Técnica de Sondeos Geotérmicos Superficiales.* Madrid: Gráficas Arias Montano S.A.

M. Bayani, C., & L. Wilson, J. (2007, VOL 43). Effects of current–bed form induced fluid flow. *WATER RESOURCES RESEARCH* .

Matthess, G., & Ubell, K. (2003). *Allgemeine Hydrogeologie-Grundwasserhaushalt.* Berlin & Stuttgart: Gebrüder Borntraeger.

Mendez Hecht, J. (2008). *Implementation and verification of the USGS solute transport code MT3DMS for groundwater heat transport modelling.* Tübingen: Eberhard Karls Universität Tübingen.

Mohnke, O. (2008). Pore size distributions and conductivities of rocks derived from Magnetic Resonance Sounding relaxation data using multi-exponential delay time inversion. *Journal of Applied Geophysics, 66* , 73-81.

Mohseni Languri, E., & Domairry Ganji, D. *Heat Transfer in Porous Media.*

Molina Giraldo, N. A. (2008). *Verification of MT3DMS as heat transport code using analytical solutions.* Tübingen: Eberhard Karls Universität Tübingen.

Molson, J. W. (1992). Thermal energy storage in an unconfined aquifer: 1. Field Injection Experiment. *WATER RESOURCES RESEARCH, VOL. 28, NO. 10* , 2845-2856.

Neuman. (1974). *Neuman*. Retrieved 5 14, 2011, from www.aqtesolv.com: http://www.aqtesolv.com/neuman.htm

Nield, D. A., & Bejan, A. (1999). *Convection in Porous Media.* New York: Springer.

Ochsner, K. (2007). *Geothermal heat pumps / Aguide to Planning and Installing.* London: Earthscan.

Pelka, W. (1983). *Heat and mass transport in saturated-unsaturated groundwater flow.* Hamburg: IHAS Publication.

Ramos Ramiz, F., & Ferrer Polo, J. (1981). *Modelación del transporte de masa en medios porosos saturados.* Valencia: Escuela técnica superior de ingenieros de Caminos, Canales y Puertos Valencia.

Rasouli, P. (2008). *Numerical Verification of Shallow Geothermal Models using FEFLOW.* Tübingen.

Regalado, C., & Carpena, R. (2004). Esimating the saturated hydraulic conductivity in a spatially variable soil with different permeameters: a stochastic Kozeny-Carman relation. *Soil and Tillage Research, 77* , 189-202.

Roscoe Moss, C. (1990). *Handbook of ground water development.* US: John Wiley & Sons.

Sanner, B. (2001). *SHALLOW GEOTHERMAL ENERGY.* Giessen, Germany: Justus-Liebig University.

Schneider, J. H. (2003). *New Least Squares Model Used For Development of Permeability-Porosity Correlation.* Poteet Texas.

Schulze-Makuch, D. (2005). *Longitudinal dispersivity data and implications for scaling behavior.* Ground Water, 43(3):.

Shaw-Yang, Y., & Hund-Der, Y. (2008). *An analytical solution for modeling thermal energy transfer.* Springer.

Shuang, J. (2009). *Geostatistical Modeling of Shallow Open Geothermal Systems.* Tübingen.

Silberstein, E. (2003). *Heat Pumps.* New York: Delmar learning.

Singhal, B., & Gupta, R. (1999). *Applied Hydrogeology of Fractured Rocks.* New York: Springer.

Vandenbohede, A., & Lebbe, L. (2010, 18). Parameter estimation based on vertical heat transport. *Hydrogeology Journal* , pp. 931-943.

Zheng, C., & Bennet, G. D. (2002). *Applied Contaminant Transport Modeling.* New York: John Wiley and Sons.

Zheng, C., & Wang, P. P. (1999). *MT3DMS Documentation and user guide.* Washington: U.S. Army Corps of Engineers.